

Annual Review of Fluid Mechanics

Supersonic Combustion in Air-Breathing Propulsion Systems for Hypersonic Flight

Javier Urzay

Center for Turbulence Research, Stanford University, Stanford, California 94305-3024;
email: jurzay@stanford.edu

Annu. Rev. Fluid Mech. 2018. 50:593–627

The *Annual Review of Fluid Mechanics* is online at fluid.annualreviews.org

<https://doi.org/10.1146/annurev-fluid-122316-045217>

Copyright © 2018 by Annual Reviews.
All rights reserved

**ANNUAL REVIEWS Further**

Click here to view this article's online features:

- Download figures as PPT slides
- Navigate linked references
- Download citations
- Explore related articles
- Search keywords

Keywords

hypersonics, compressible flows, turbulent combustion, scramjets, high-speed chemical propulsion, sound barrier

Abstract

Great efforts have been dedicated during the last decades to the research and development of hypersonic aircrafts that can fly at several times the speed of sound. These aerospace vehicles have revolutionary applications in national security as advanced hypersonic weapons, in space exploration as reusable stages for access to low Earth orbit, and in commercial aviation as fast long-range methods for air transportation of passengers around the globe. This review addresses the topic of supersonic combustion, which represents the central physical process that enables scramjet hypersonic propulsion systems to accelerate aircrafts to ultra-high speeds. The description focuses on recent experimental flights and ground-based research programs and highlights associated fundamental flow physics, subgrid-scale model development, and full-system numerical simulations.

1. INTRODUCTION

The year 2017 marked the seventieth anniversary of the breaking of the sound barrier by US Air Force (USAF) General Charles E. “Chuck” Yeager aboard the Bell X-1 experimental aircraft. This event marked a significant milestone in aeronautics and greatly enhanced our collective comprehension of transonic aerodynamics. The X-1 was powered by four rocket engines buried within the rounded, orange fuselage (**Figure 1a**), which provided the aircraft with a burning time of just a few minutes after a drop launch from the bomb bay of a B-52 mother ship. Several experimental planes soon followed the X-1 that expanded the frontiers of supersonic flight. The most acclaimed was the rocket-powered North American X-15, which in 1967 crossed the skies at Mach 6.7 (**Figure 1b**). Fifty-one years later, the X-15 still retains the undisputed world record for the highest speed ever reached by a manned, powered, winged aircraft.

It is a testament to the staggering difficulty of the endeavor that even 70 years after the breaking of the sound barrier, attaining stable long-range manned hypersonic flight ($Mach > 5$) continues to outstrip humankind’s determination in its quest to discover faster methods of air transportation. The gas environment around a hypersonic aircraft is one in which the extreme temperatures and intense aerothermal loads, caused by air friction and shock waves, continuously endanger the maneuverability and structural integrity of the vehicle. In addition to the challenges associated with structural design, thermal protection, and aerodynamic trim, several remaining pieces of the puzzle of hypersonic flight relate to the stringency of the technical requirements in the chemical propulsion systems needed to efficiently reach hypersonic speeds.

The rocket engines in the X-1 and X-15 planes imposed constraints on flight parameters resulting in limited ranges and short burning times that deterred using the technology in practical scenarios. An important disadvantage of rocket-based propulsion systems is the burden of having to dedicate thrust to accelerate the oxidizer carried onboard. For instance, the oxidizer load in

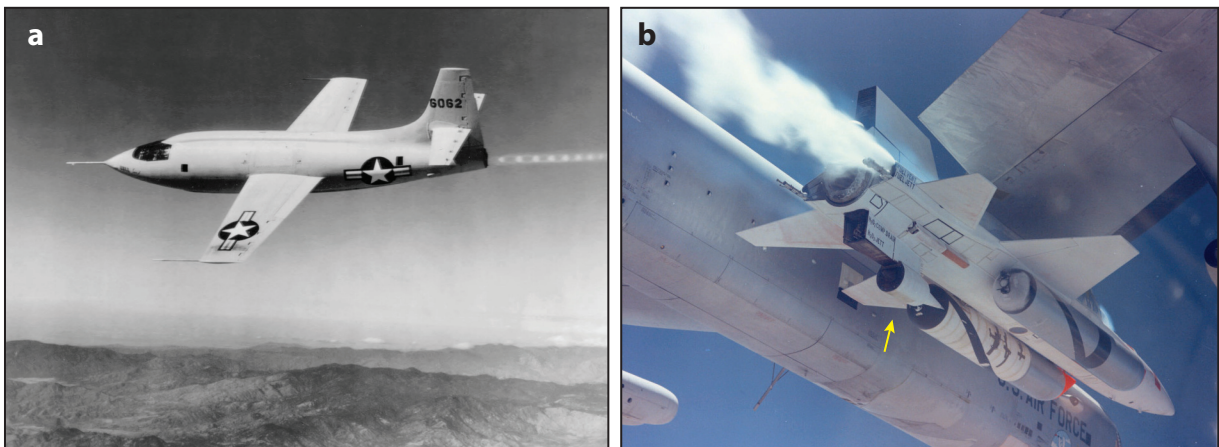


Figure 1

(a) Bell X-1 streaking across the skies during the first flight to break the sound barrier on October 14, 1947. Reproduced with permission of C.E. Yeager, copyright <http://www.chuckyeager.com>. (b) X-15-A2 drop-launched from a B-52 Stratofortress into its last and record-breaking Mach-6.7 hypersonic flight on October 3, 1967. In this flight, the X-15-A2 carried a mock-up version of the Hypersonic Research Engine (yellow arrow) in preparation for future, Mach-8+ flights using scramjet technology. However, the engine pylon suffered severe structural damage caused by shock interference heating during the flight (Watts 1968), which, in addition to intense charring in several other parts of the fuselage, rendered the airplane irreparable and prompted the termination of the program in 1968. Courtesy of the National Museum of the US Air Force.

the X-15 translated to approximately 39% of the 14.2-ton gross weight at drop launch. In rockets such as the SpaceX Falcon-9, lifting 23 tons of payload to low Earth orbit (LEO) requires 549 tons of gross weight at the launch pad, 65% of which approximately corresponds to the weight of the liquid oxygen. In a current commercial landscape of rocket space launchers where the cost per kilogram of the payload sent to LEO is in the range of US\$1,000–20,000, an attractive solution to the problem is to use air-breathing engines in which the oxidizer is supplied by the surrounding air and mixed in a combustor with the fuel carried onboard.

Hypersonic air-breathing vehicles provide the potential for fast long-range civil transport around the globe, long-distance fast strike capabilities for defense systems, and high-launch-rate space transportation of payloads to LEO (**Figure 2a**). However, exiting the atmosphere is not possible due to oxidizer starvation, and transition at Mach 10–12 to a second, rocket-based stage is required to accelerate the payload across the mesopause to hypervelocities of order Mach 20–25 in order to achieve LEO altitudes and orbital injection energies. The resulting hypersonic spaceplane concept is typically one with an operational empty weight similar to an LEO rocket launch system with a payload installed, but which has a much smaller total gross weight in the range of 100–200 tons enabled by the smaller amount of oxidizer carried onboard. Unfortunately, these advantages are counterbalanced by outstanding technical difficulties associated with the air-breathing propulsion system in capturing atmospheric air and burning it in the combustor at flight speeds of order 6,000–10,000 km/h.

The energy released in the combustor of hypersonic air-breathing engines must be large enough to generate thrust and overcome the external drag on the vehicle and the internal drag caused by the friction of the ingested air through the engine. However, the drag forces increase with the flight speed, and the resulting increasingly short residence times of the airflow in the combustor tend to suppress the aerodynamic processes essential for mixing and combustion.

Turbojets and turbofans, typically used in airliners and fighter aircrafts at moderate speeds, use rotating compressors to pressurize and slow down the airflow to subsonic velocities to enable combustion and produce thrust. The stabilization of combustion processes in these systems relies on swirl breakdown and low-speed flame propagation mechanisms that are relatively well known. At supersonic speeds, the dynamic compression and deceleration of the airflow can be efficiently achieved by augmenting turbojets with variable-geometry intakes, air-bleeding systems, and afterburners to switch from turbojet to ramjet modes, as in the Pratt & Whitney J-58 turboramjet engines of the Lockheed SR-71 Blackbird aircraft, which was capable of flying at Mach 3.2. At even higher speeds entering in the hypersonic range, the deceleration of the airflow to subsonic velocities leads to untenable energy losses and large thermal loads that prohibit the use of these classical propulsion systems.

An alternative to circumvent these limitations is provided by a different class of engines termed supersonic combustion ramjets (scramjets). In scramjets, the airflow is compressed dynamically through an intake system integrated in the forebody that does not require rotating elements, and the fuel and oxidizer are burnt under supersonic velocity conditions in the combustor (**Figure 2b**). However, at such high speeds, mixing and combustion processes cannot easily fit within the combustor length because the total residence time available for reactants to burn is typically a fraction of a millisecond with supersonic flow throughout. The fuel, which is injected in the combustor through a separate port, needs to be mixed at the molecular level with the oxygen present in the ingested airflow for combustion chemical reactions to occur. Sufficient residence time must therefore be allotted for large-scale turbulent structures in shear layers to grow and cascade into smaller eddies that trigger microscale mixing between reactants. Attenuation of this growth rate occurs at supersonic speeds due to compressibility effects that slow down the required mixing. Eventually, the fuel and oxidizer burn upon mixing in a sequence of chemical reactions

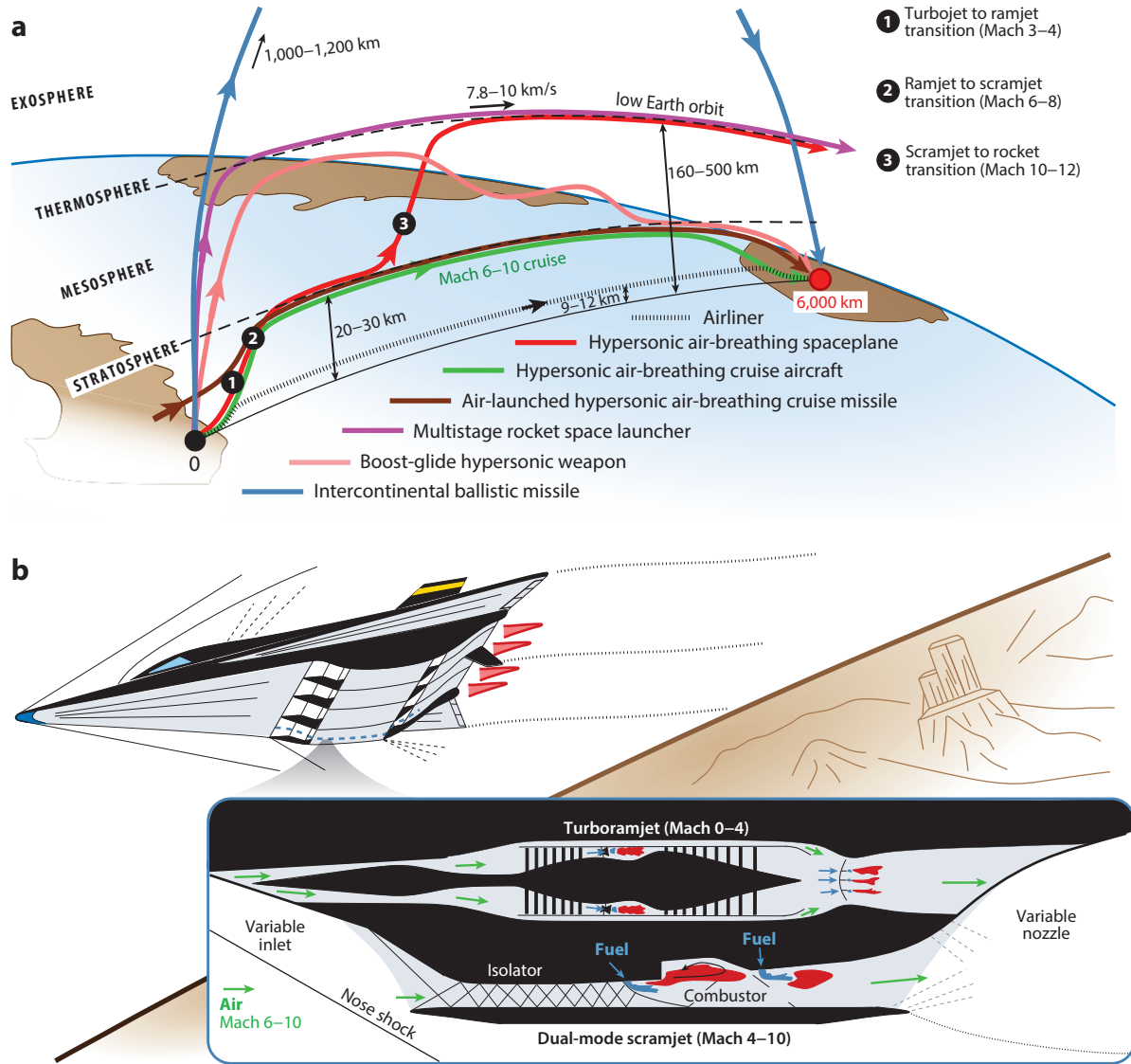


Figure 2

(a) Characteristic flight trajectories for different aerospace systems including hypersonic scramjet-powered air-breathing vehicles.
 (b) Notional hypersonic air-breathing aircraft including a variable-geometry, combined-cycle propulsion system composed of a turboramjet (Mach 0-4) along with a dual-mode scramjet that can operate both as a ramjet (Mach 4-6) with subsonic combustion and as a scramjet (Mach 6-10) with supersonic combustion.

whose initiation is often enabled by hot temperatures of order 1,000–1,400 K caused by the partial deceleration of the airflow while it flows through a number of shock waves inside the engine. Typical autoignition times in these conditions are of order 10–100 μ s, indicating that a significant fraction of the flow path in the combustor is to remain chemically frozen unless modifications are made to enable longer residence times and robust flame-anchoring mechanisms. To summarize, the challenge of enterprise supersonic combustion in scramjets is—in lay terms—as difficult as lighting a match in a hurricane.

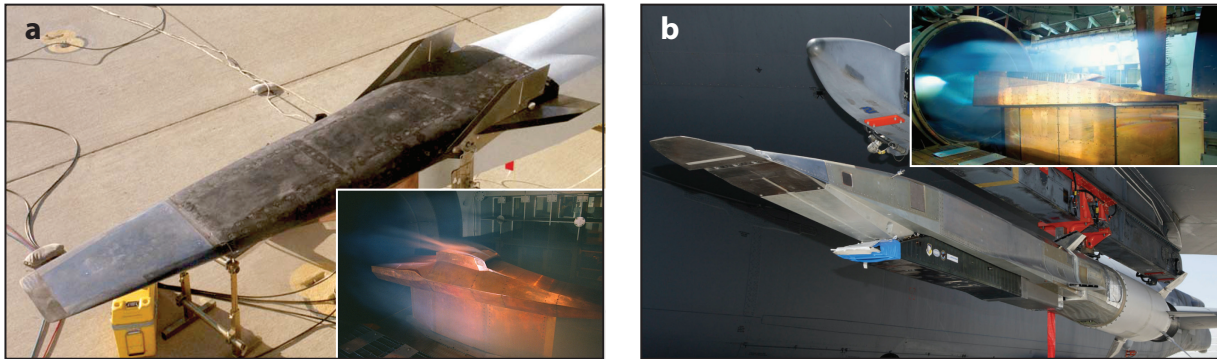


Figure 3

(a) X-43A and (b) X-51A on the tarmac before flight. (*Insets*) Corresponding scramjet tests at NASA-LaRC. Images are US Government work not subject to copyright in the United States. Adapted from Marshall et al. (2005) and Hank et al. (2008).

This review focuses on supersonic combustion phenomena in scramjets. It builds on two preceding reviews in this journal by Ferri (1973) and Curran et al. (1996) on the same topic, summarizing part of the new knowledge acquired by the community in the last few decades. The remainder of this article is organized as follows. Section 2 provides a brief summary of recent scramjet propulsion research programs. Section 3 describes the character of supersonic combustion, including associated flow physics, modeling, and computations. Lastly, Section 4 closes with conclusions and future prospectives.

2. SCRAMJET PROPULSION RESEARCH PROGRAMS

Several scramjet research programs developed in the last 50 years deserve discussion, but it is not the purpose of this section to provide a complete historical account. Details about early pioneering US projects such as the Hypersonic Research Engine (1964–1975), which aimed at extending the capabilities of the X-15 to velocities beyond Mach 8 (Figure 1b), or the National Aero-Space Plane (NASP; 1986–1993) under the Reagan administration, which attempted the design and construction of the Rockwell X-30 passenger spaceliner, can be found in a seminal review by Hallion (1987). Additionally, the reference monographs by Heiser & Pratt (1994) and Curran & Murthy (2000) provide thorough descriptions of scramjet research programs in the United States, Russia, Germany, Japan, Australia, and France. Also included in those references are details of the NASA's Hyper-X project (McClinton 2006) that started in the wake of NASP and culminated later in 2004 with the Mach-9.6 flight of the unmanned X-43A hypersonic aircraft (Figure 3a).

The focus here is on summarizing the characteristics of a few recent programs that have inspired configurations often used by the scientific community as benchmarks for theories, experiments, and computations reported in the open literature, as described in Section 3. Remarkably, some of these innovative programs have broken the limitations of traditional ground-based testing by using sounding rockets to obtain *in situ* flight data of supersonic combustion phenomena in scramjets, as highlighted in Sections 2.2 and 2.3.

2.1. The Role of Hypersonic Air-Breathing Propulsion in National Security

Much of the field of supersonic combustion in hypersonic air-breathing engines has been traditionally shielded behind classification because of its applications for national security. The situation is

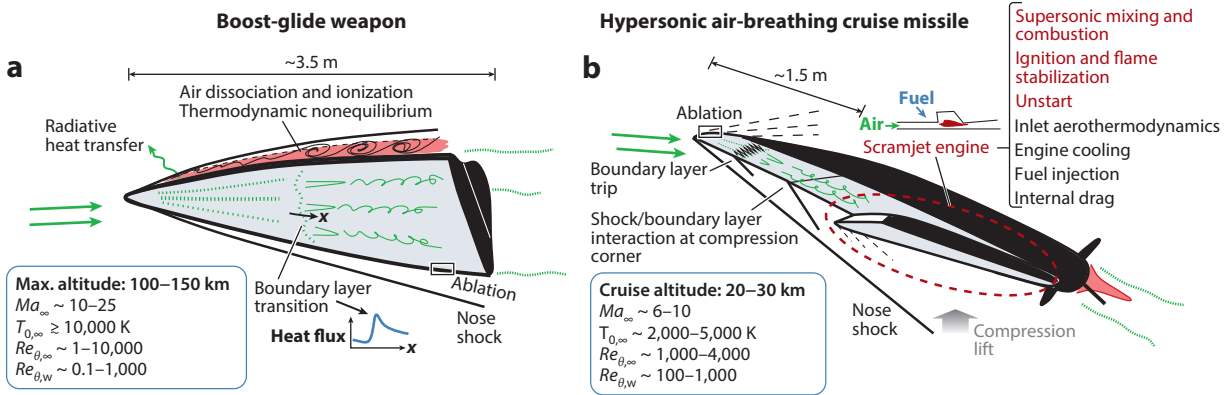


Figure 4

Flow physics of (a) boost-glide weapons and (b) hypersonic air-breathing cruise missiles. Estimates of flight Mach numbers (Ma_∞), stagnation temperatures ($T_{0,\infty}$), free stream-based ($Re_{\theta,\infty}$) and wall recovery temperature-based ($Re_{\theta,w}$) momentum thickness Reynolds numbers are made using a recovery factor of 0.8, indicated lengths, and the US Standard Atmosphere.

perhaps best pictured by paraphrasing Wernher von Braun in reference to his work during World War II on missiles that preceded today's space rockets: "It seems that this is another demonstration of the sad fact that so often important new developments get nowhere until they are first applied as weapons" (Huzel 1962, p. 119).

The paradigms of stealth and precision that have dominated weaponry design in the last decades of the twentieth century, such as the Lockheed F-117 and Northrop Grumman B-2 aircrafts, are now gradually shifting toward a framework of rapid unfolding of events by the expeditious destruction of targets located anywhere in the world using prompt global strike (PGS) hypersonic weaponry, including hypersonic fighter aircrafts and unmanned aerial vehicles, along with hypersonic precision-guided maneuverable missiles carrying conventional or no warheads at all (Hallion et al. 2016). The high speeds and in-flight controllability of advanced PGS hypersonic weapons would make these extremely difficult to intercept using traditional countermeasures such as surface-to-air missiles and would not require the use of forward-based forces.

Hypersonic military technology programs have traditionally been subdivided into transatmospheric and endoatmospheric vehicle concepts. From a fluid mechanical standpoint, the problems associated with each type are fundamentally different (Figure 4). Recent research programs have investigated transatmospheric boost-glide weapons (Figures 2a and 4a) that are rocket-boosted to orbital or suborbital altitudes and left to glide hypersonically back into the atmosphere to impact targets [e.g., see DARPA (Defense Advanced Research Projects Agency)/USAF's Falcon project in Walker et al. (2008)]. In these concepts, the aerothermodynamics of external hypersonic boundary layers play a crucial role in predicting thermomechanical loads during reentry and gliding at speeds of order Mach 10–25. Outstanding problems include determining the laminar-to-turbulence transition region emerging during reentry that is responsible for a large increase in localized heat transfer to the airframe; the treatment of dissociation, ionization, and thermodynamic nonequilibrium effects in boundary layers as a result of the large stagnation temperatures involved; and the computation of radiative heat transfer on thermal-protection surfaces. The reader is referred to a recent review by Leyva (2017) that describes unsolved issues in fundamental hypersonic aerothermodynamics.

Endoatmospheric vehicles, in contrast, follow hypersonic cruising trajectories in the stratosphere at lower Mach numbers of order 6–10 (Figures 2a and 4b), which lead to more manageable

thermomechanical loads and lesser radiative, thermodynamic, and chemical nonequilibrium effects. However, they require a continuous supply of thrust, which is envisioned to be produced by scramjets, as in the Boeing X-51A flight demonstrator (**Figure 3b**) (Hank et al. 2008). Such missile concepts have intercontinental range following precision-guided maneuverable trajectories that minimize collateral damage and have arrival times of less than an hour. These are important advantages over other alternatives for PGS warfare because weapons following partial or complete suborbital trajectories might be confused in early warning systems with currently stockpiled intercontinental ballistic missiles carrying nuclear warheads, which could trigger a large-scale nuclear conflict (Woolf 2016). This has been referred to as the warhead ambiguity problem and is a relevant technical design factor currently under scrutiny (Natl. Res. Counc. 2008). Additionally, there are a number of outstanding fluid mechanical problems associated with these devices. Some pertain to external aerodynamics and the generation of lift with minimal winged surface area to minimize the aeroheating of leading edges. A solution to this is the waverider concept that has been investigated in the X-51A, which generates compression lift through an external oblique shock that emanates from the spatular nose and also serves to dynamically pressurize the airflow entering the scramjet engine. Furthermore, and in stark contrast to subsonic propulsion systems such as turbofan engines in airliners, the scramjet engine must be aerodynamically integrated in the airframe to avoid thrust penalties and intense aeroheating due to exceedingly large drag forces on salient features from the fuselage.

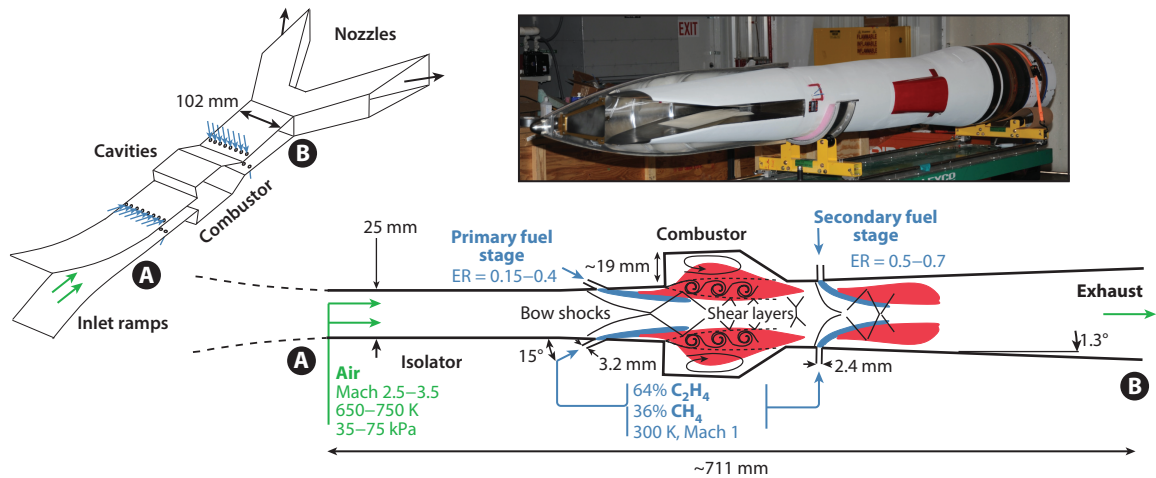
A central challenge for hypersonic air-breathing aircrafts and missiles consists of attaining stable supersonic combustion in the scramjet in order to produce continuous and sufficient thrust to overcome all drag forces. However, this is an unsolved problem whose urgency in many cases supersedes all other aerothermal constraints outlined above. Most recently, in 2013, the X-51A successfully flew at Mach 5.1 on scramjet power for 210 s (i.e., approximately 6% of the total flight path in **Figure 2a**), but it also suffered a catastrophic unstart malfunction during its second flight in 2011. Unstart is a poorly understood phenomenon closely related to the dynamics of fuel injection and combustion that is discussed in Section 3.2.3.

2.2. The HIFiRE Flight Experiments

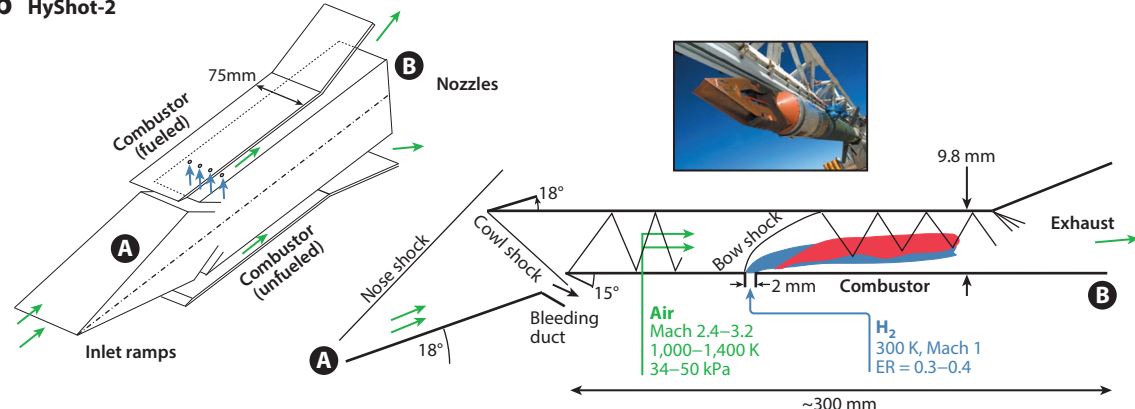
One of the most acclaimed programs on hypersonics in recent years has been HIFiRE (Hypersonic International Flight Research Experimentation), which is jointly operated by AFRL (the US Airforce Research Laboratory), AFOSR (the Airforce Office of Scientific Research), NASA, ATK-GASL (Alliant Techsystems' General Applied Science Laboratory), and Australia's Defense Science and Technology Group, and whose objective is the fundamental understanding of hypersonic flight phenomena in support of the X-51A (Bowcutt et al. 2012). Two flights of the program, HIFiRE-2 and -3, have been devoted to investigating supersonic combustion in scramjets.

The HIFiRE-2 configuration was successfully flown in 2012 and consisted of a hydrocarbon-fueled, dual-mode, Mach-8+ scramjet mounted on a sounding rocket (**Figure 5a**). An overview of the flight experiment was provided by Jackson et al. (2014). The combustor had two opposed cavity-based flameholders that enabled combustion stabilization and dual-mode transition, the latter corresponding to the transition between subsonic (ramjet) to supersonic (scramjet) modes as the flight Mach number increased from 6 to 8. Two sets of fuel injectors, corresponding to the primary and secondary stages upstream and downstream of the cavity, respectively, supplied a gaseous mixture made up of 64% ethylene (C_2H_4) and 36% methane (CH_4) content by volume. At Mach 6.0 and 23.2-km altitude during ascent, the scramjet was ignited and kept burning for 13 s thereafter. During that period, the primary and secondary fuel mass flow rates were increased

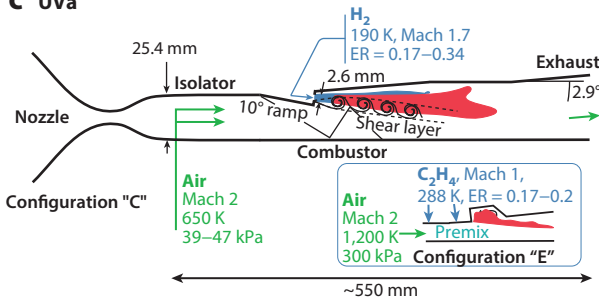
a HIFIRE-2



b HyShot-2



c UVa



d DLR

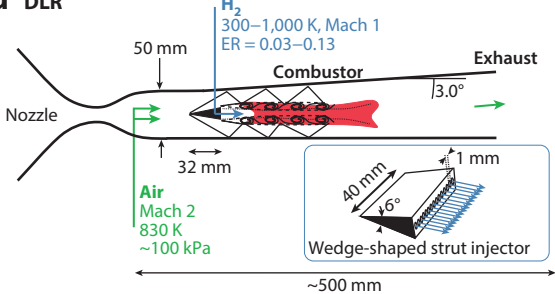


Figure 5

Scramjet configurations (not to scale) of (a) HIFIRE-2, (b) HyShot-2, (c) UVa, and (d) DLR experiments. In panel *a*, the parameters correspond approximately to ground test conditions (M. Gruber, personal communication). Readers are referred to program overviews for details (Waidmann et al. 1995, Smart et al. 2008, McDaniel et al. 2009, Jackson et al. 2014). Insets in panels *a* and *b* reprinted with permission of M. Gruber and M. Smart, respectively. Abbreviations: DLR, German Aerospace Center; ER, equivalence ratio; HIFIRE, Hypersonic International Flight Research Experimentation; UVa, University of Virginia.

linearly in time until achieving their scheduled equivalence ratios of 0.4 and 0.6, respectively. References to the equivalence ratio, $ER = (s/Y_{O_2,A})(\dot{m}_F/\dot{m}_A)$, as a characteristic fueling rate parameter are often found in scramjet-related literature, where s is the mass of oxygen burnt per unit mass of fuel in stoichiometric proportions, $Y_{O_2,A} = 0.23$ is the mass fraction of oxygen in air, and \dot{m}_F and \dot{m}_A are the mass flow rates of fuel and air, respectively.

The HIFIRE-2 scramjet incorporated pressure and temperature sensors on the walls, along with tunable diode-laser absorption spectroscopy (TDLAS) (Liu et al. 2005) to measure spatiotemporal distributions of temperature and water vapor concentration in the burnt gases at the combustor exit. As of the date of publication of this article, however, the data acquired during the flight test are of limited distribution and have not been released to the public. Instead, data sets from ground-based tests are available (Cabell et al. 2011) along with a large number of supporting experiments on cavity-based scramjets at the AFRL (Gruber et al. 2004, Mathur et al. 2001, Tuttle et al. 2014, Gradya et al. 2016, Ombrello et al. 2016). Additional aspects of these configurations, along with accompanying full-engine simulations, are described in Section 3.

The HIFIRE-3 configuration was successfully flown in 2012 but has been much less reported in the open literature. It consisted of an axisymmetric, hydrogen-fueled, Mach-8 scramjet mounted on a sounding rocket and was ignited during a ballistic descent (Bowcutt et al. 2012). The fuel was injected at a conical, inward-turning airflow inlet under mild temperature conditions that prevented autoignition, and the combustor was not equipped with any flameholder. Instead, the objective of the flight was to assess the mechanism of radical farming (McGuire et al. 2008), by which the sole action of a shock train is responsible for igniting the fuel–oxidizer mixture and releasing chemical heat, as described in Section 3.1.4. Ground-based experiments have been reported that confirm the feasibility of the concept (Boyce et al. 2010), which has been later pursued in the sequel project SCRAMSPACE on a similar configuration (Tirtey et al. 2014).

2.3. The HyShot Flight Experiments

The HyShot program is a University of Queensland initiative that has delivered four flight tests of scramjets using sounding rockets (Smart et al. 2008). An overview and data analysis of the second flight, HyShot-2, are provided by Smart et al. (2006).

The HyShot-2 scramjet configuration consisted of a double-wedge intake and two back-to-back constant-area hydrogen-fueled combustors (**Figure 5b**). The large deflection angle of the first wedge ensured the proper increase of temperature and pressure to favor conditions for ignition. The shock emerging from the cowl wedge, along with the boundary layer formed on the leading wedge, was bled in a shock trap located along the flow path upstream from the entrance to the combustors. One of the combustors remained unfueled during the flight, and the other was fueled with gaseous hydrogen injected in the form of a sonic jet in crossflow normal to the supersonic air stream with an equivalence ratio of 0.34. The fueled combustor was ignited at 35-km altitude when the payload was descending at Mach 7.6 and burned for an additional 6 s. Because of nutation and rolling motions created by aerodynamic forces, the fueled combustor was subject to variable angles of attack as it alternated between windward and leeward sides on descent. Nevertheless, pressure measurements from transducers on the combustor walls demonstrated the persistence of supersonic combustion as manifested by a ramp in pressure that is characteristic of supersonic flows under heat addition (**Figure 6a**). The flight provided a data set that, in conjunction with ground-based tests (Paull et al. 2000, Gardner et al. 2005, Laurence et al. 2013), has proved useful in understanding complex effects and enabled a platform for comparisons with full-system simulations, as shown in Sections 3.2.2 and 3.2.3.

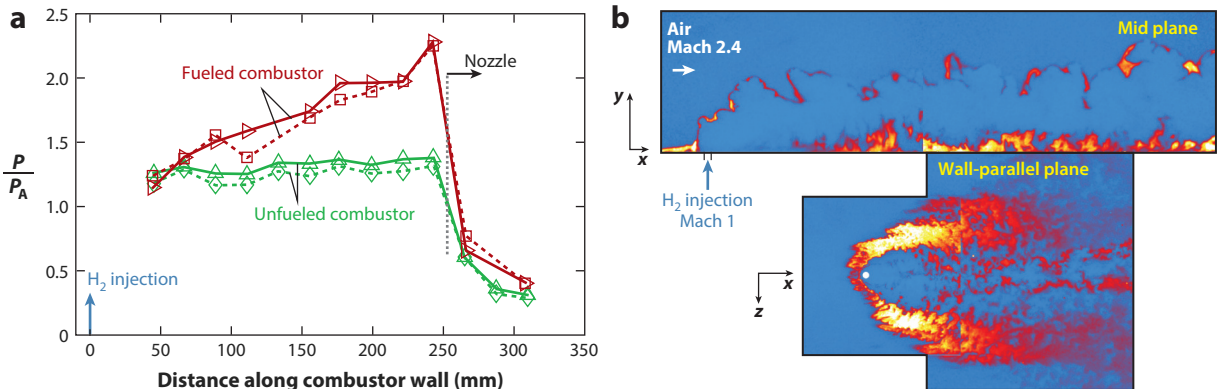


Figure 6

(a) Static pressure measurements along the HyShot-2 combustor wall in the fueled and unfueled sides at two different time instants during flight (*solid and dashed lines*) and normalized with the value of the static pressure at the combustor entrance P_A . Based on Smart et al. (2008). (b) OH-planar laser-induced fluorescence images of supersonic flames in the Stanford High Temperature Gasdynamics Laboratory scramjet model combustor on the mid-plane (*top*) and on a wall-parallel plane at $y = 0.5d$ (*bottom*), where d is the diameter of the injection orifice. Adapted with permission from Gamba & Mungal (2015).

2.4. Ground-Based Testing Programs

Several scramjet propulsion research programs have recently been completed that did not involve flight testing but provided important insight into supersonic combustion physics. Some of these programs are highlighted below, although this list is by no means exhaustive.

The US National Center for Hypersonic Combined-Cycle Propulsion at the University of Virginia (UVA) has addressed physical and engineering aspects of acceleration of aircrafts from subsonic to hypersonic speeds (McDaniel et al. 2009). From a propulsion standpoint, this requires transition from turbojet to ramjet at Mach 3–4, and from ramjet to scramjet at Mach 6–8. Whereas the former necessitates alternation between flow paths using variable-geometry intakes and nozzles (Figure 2*b*), the latter involves dual-mode transition in a fixed scramjet geometry by varying the fuel flow rate, as demonstrated in HIFiRE-2.

UVA's scramjet used for investigating dual-mode transition was a direct-connect rig composed of a converging-diverging nozzle that delivered an electrically preheated Mach-2 airflow into the combustor (Figure 5*c*). Different geometrical variants of this scramjet have been studied, including configurations C and E where a constant-area extension of the combustor, relative to a shorter configuration A, facilitated thermal choking at high fuel flow rates and controllably unstarted the engine to transition from ramjet to scramjet modes (Fulton et al. 2013). Both configurations A and C employed H₂ fuel provided by a wall-mounted compression-ramp injector (Goyne et al. 2006, McRae et al. 2013). In configuration E, C₂H₄ was injected far upstream into the isolator to create premixing with the airflow and to study premixed combustion in the cavity shear layer (Cantu et al. 2016).

Scramjet combustor geometries with parallel injection of fuel in the direction of the airflow have been investigated at the German Aerospace Center (DLR) (Waidmann et al. 1994, 1995). The DLR scramjet facility consisted of a converging-diverging nozzle that provided a Mach-2 airflow into a combustor in which the upper wall was slightly divergent (Figure 5*d*). Hydrogen was injected through 15 holes carved in the afterbody of a two-dimensional (2D) wedge-shaped strut located mid-distance from the upper and bottom walls of the combustor. Pressure transducers and nonintrusive optical techniques were employed to study the flow fields. The airflow temperature

was too low to enable lifted autoignition. Conversely, the flame was stabilized in the recirculation zones downstream of the wedge. OH-based diagnostics suggested that the burning rate of the diffusion flames was strengthened at locations where shocks impinged on the mixing layer. A similar configuration has been studied in a joint project by the French Aerospace Agency (ONERA) and the Japanese Aerospace Exploration Agency (JAXA) using a scramjet combustor supplied with wedge-shaped strut injectors alternating in shape to generate counterrotating streamwise vortices that enhance mixing and combustion (Scherrer et al. 2016).

Other relevant measurements were made by Gamba & Mungal (2015) in a hydrogen-fueled jet-in-crossflow model scramjet at Stanford's High Temperature Gasdynamics Laboratory (HTGL) as part of the Predictive Science Academic Alliance Program (**Figure 6b**). These measurements illustrated a variety of supersonic flame structures as a function of the jet-to-free stream momentum ratio and highlighted the importance of the near-wall recirculation regions induced by the jet in stabilizing the flame.

3. SUPERSONIC COMBUSTION PHYSICS AND COMPUTATION

Given the extreme flow velocities of order 1,000–3,000 m/s and the complexities in the physics of the compressible turbulent reacting flows that prevail in the configurations described above, it is not surprising that supersonic combustion in scramjet engines is a relatively less understood problem in combustion science than those addressing low-speed phenomena. Most foundational supersonic combustion models have relied heavily on inviscid, steady-state 1D streamtube formulations of compressible reacting flows incorporating volume-averaged heat release. Extensive reviews of these models are provided by Ferri (1973), Curran et al. (1996), Heiser & Pratt (1994), and Curran & Murthy (2000). Instead, the focus of this section is on summarizing the main physical aspects associated with supersonic combustion physics, including progress on numerical simulations of full systems.

3.1. Physical Characteristics of Supersonic Combustion

Combustion in most scramjet engines is conditioned by two important characteristics readily observed in **Figure 5**. The first one is that, in most configurations, the fuel and oxidizer flow separately into the combustor. The second is that the characteristic velocities involved in the fuel and oxidizer free streams are two to three orders of magnitude larger than typical premixed flame propagation speeds $S_L \sim 0.3\text{--}3$ m/s. Although partial premixing of reactants is expected upstream of the ignition zones, it is conceptually plausible to assume that the most frequent mode of combustion downstream is the nonpremixed one. However, this is not to say that premixed combustion is irrelevant in scramjets. Experimental observations have frequently pointed to that mode as responsible for combustion stabilization in recirculation zones or near walls where the flow velocities may be sufficiently small to support deflagrations (Micka & Driscoll 2009, Cantu et al. 2016). Despite this multimodal combustion character and other complicating effects often observed such as turbulence and compressibility, it is convenient to consider first the canonical configuration of the high-speed coflow laminar diffusion flame sketched in **Figure 7a**, in which the air and fuel stream velocities U_A and U_F are much larger than S_L .

The structure of diffusion flames dates back to the work of Burke & Schumann (1928) and has been the subject of a separate review (Liñán et al. 2015). Early analyses established that a solution exists in the infinitely fast chemistry limit in which the description is independent of the chemical kinetics. In this limit, the local chemical time $t_{ch} \sim B^{-1}e^{T_a/T}$, which depends on the temperature T , the frequency factor B , and the activation temperature T_a of the overall chemical step, is much

smaller than the molecular diffusion time across the coflow mixing layer $t_d \sim \delta^2/D_F$, where δ and D_F denote the local mixing layer thickness and the fuel mass diffusivity, respectively. In this way, the flow remains in chemical equilibrium on both sides of an infinitesimally thin reaction sheet that separates fuel-only ($Y_{O_2} = 0$) and oxidizer-only ($Y_F = 0$) regions. Observations indicate that this regime of large Damköhler numbers $Da = t_d/t_{ch} \rightarrow \infty$, which is often referred to as diffusion- or mixing-controlled combustion because the reactants burn upon molecular mixing, is a relevant one for supersonic combustion in scramjets, at least in an idealized sense (Liñán et al. 1966, Ferri 1973). Close to the injector, however, both time scales become of the same order, giving rise to a chemically frozen region that is characterized by mixing without reaction and is followed downstream by an ignition front.

The ignition of diffusion flames in high-speed coflow mixing layers was studied by Liñán & Crespo (1976) following the simplified framework in which the overall activation energy is large in the sense that T_a/T_A is a large parameter, where T_A is the temperature of the air coflow. In this limit, the chemical reaction rate, which contains an Arrhenius exponential factor of the form $\exp(-T_a/T_A)\exp[T_a(T - T_A)/(TT_A)]$, becomes largely intensified even under small relative temperature increments of order T_A/T_a . As a result, small temperature variations lead to a well-defined thermal runaway by which the temperature disturbance precipitously diverges at distances of order $L_{ig} \sim U_A t_{ig}$ from the orifice, where t_{ig} is an ignition time that is obtained from the numerical integration of the second approximation for the temperature and is of the same order as both the local diffusion time t_d and the homogeneous explosion time based on T_A . The resulting ignition kernel does not rely on streamwise molecular diffusion for its stabilization, as opposed to low-speed triple flames. However, it also resembles a tribrachial structure composed of rich and lean deflagrations along with a trailing diffusion flame located along the stoichiometric surface. Most notably, the two deflagrations are highly slanted at angles $\alpha \sim S_L/U_A \ll 1$ in order to compensate for the high speed of the flow in comparison with the laminar premixed flame speed.

The effects of a strain rate A on laminar diffusion flames in counterflow mixing layers were addressed by Liñán (1974), who employed matched asymptotic expansions in the aforementioned limit of large activation energies to obtain the characteristic S-shaped curve (**Figure 7c**). The upper branch of this curve describes the limit of vigorously burning flames or the mixing-controlled regime, in which the chemical time t_{ch} is much shorter than the straining time A^{-1} and reactants become depleted very quickly as they diffuse through the mixing layer. Similarly, a lower branch describes the chemically frozen mixing of fuel and oxidizer, with $t_{ch} \gg A^{-1}$. The intermediate branch represents an unstable partial-burning regime in which one of the reactants leaks abundantly through the flame. The upper and lower turning points, which are representative of extinction and ignition, respectively, correspond to abrupt quasi-static phenomena caused by finite-rate chemistry but with no temporal dynamics associated with them because the formulation corresponds to an elliptic boundary value problem. This is in contrast with the analysis of the unstrained coflow mixing layer by Liñán & Crespo (1976) mentioned above, which corresponds to a parabolic problem in space (in the laboratory frame) or in time (in the relative frame moving at the mean speed) and therefore accounts for the spatiotemporal development of the ignition process.

The canonical laminar structures described above represent the conceptual core of widely used subgrid-scale (SGS) models for large-eddy simulations (LES) of turbulent combustion, such as the flamelet models (Peters 2000). These models are based on the hypothesis that there is an asymptotically large separation of scales whereby a turbulent diffusion flame can be decomposed into laminar flames subject to a local counterflow strain rate A emerging from the strain-rate-containing turbulence microscales (**Figure 7b**). LES modeling strategies for turbulent supersonic combustion are discussed in Section 3.2.

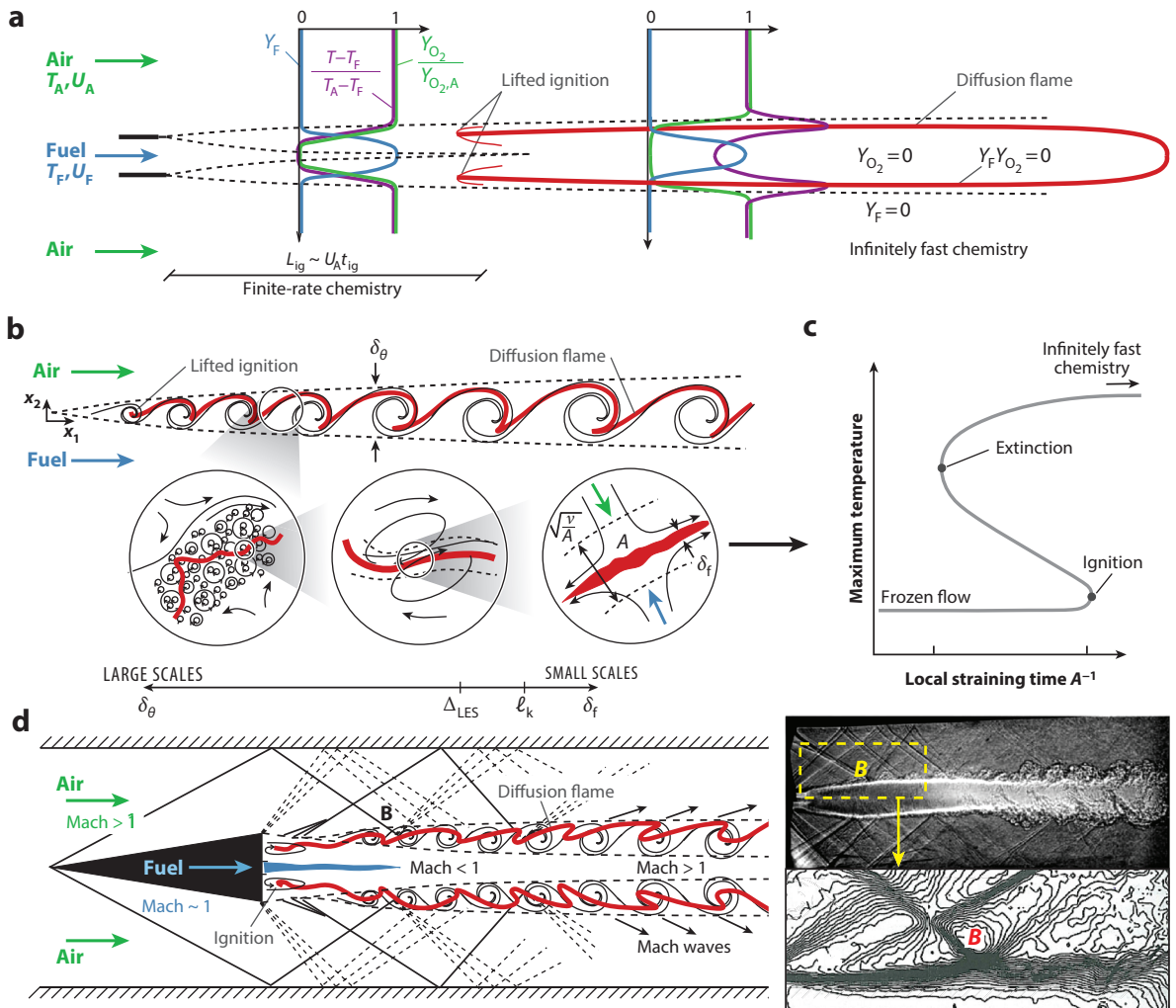


Figure 7

(a) Laminar diffusion flame in a high-speed coflow. (b) Flamelet model for turbulent diffusion flames. (c) S curve for laminar counterflow diffusion flames. (d) Schematics of the flow in the DLR (German Aerospace Center) scramjet (**Figure 5d**), along with a shadowgraph (*top*) and Rayleigh-scattering iso-density lines (*bottom*) showing a combustor cross section and the shock/mixing-layer interaction region at *B*. Adapted with permission from DLR (Waidmann et al. 1994, 1995).

Practical supersonic combustion problems pose significant challenges to these canonical structures. The discussion is best motivated by comparing the laminar coflow or counterflow simplified problems with that of **Figure 7d**, which depicts the turbulent supersonic reacting flow in the DLR scramjet, whose particular operation parameters are shown in **Figure 5d**. Additional effects arise in the latter that are inherent to most practical supersonic combustion problems. These include complex transport and chemical kinetics, compressible turbulence and mixing, flow recirculation, shock-induced combustion, thermal choking, and near-wall burning. A brief summary of these phenomena is given in Sections 3.1.2–3.1.5 and 3.2.3, beginning with a general formulation for later use in the text.

3.1.1. Conservation equations for supersonic combustion. In supersonic combustion calculations, the flow field is described by the Navier–Stokes and species conservation equations

$$\frac{\partial \rho}{\partial t} + \nabla \cdot (\rho \mathbf{u}) = 0, \quad 1.$$

$$\frac{\partial \rho \mathbf{u}}{\partial t} + \nabla \cdot (\rho \mathbf{u} \mathbf{u}) = -\nabla P + \nabla \cdot \boldsymbol{\tau}, \quad 2.$$

$$\frac{\partial \rho e_t}{\partial t} + \nabla \cdot (\rho \mathbf{u} e_t) = -\nabla \cdot (P \mathbf{u}) + \nabla \cdot (\boldsymbol{\tau} \cdot \mathbf{u}) - \nabla \cdot \mathbf{q}, \quad 3.$$

$$\frac{\partial \rho Y_i}{\partial t} + \nabla \cdot (\rho \mathbf{u} Y_i) = -\nabla \cdot (\rho \mathbf{V}_i Y_i) + \dot{w}_i, \quad i = 1, \dots, N, \quad 4.$$

along with the equation of state $P = \rho R_g T$. In this formulation, \mathbf{u} is the velocity vector; $R_g = R^0/W$ is the gas constant; W is the average molecular weight; $e_t = |\mathbf{u}^2|/2 + \sum_{i=1}^N (b_i^0 + b_i) Y_i - P/\rho$ is the total specific energy; Y_i is the mass fraction; b_i^0 is the formation enthalpy; $b_i = \int_{T^0}^T c_{pi} dT$ is the partial specific enthalpy; c_{pi} is the specific heat; N is the number of species; and P , ρ , and T are the static values of pressure, density, and temperature, respectively. Similarly, $\boldsymbol{\tau} = 2\mu[\mathbf{S} - (\nabla \cdot \mathbf{u})\mathbf{I}/3]$ is the viscous stress tensor, where μ is the molecular viscosity and $\mathbf{S} = (1/2)(\nabla \mathbf{u} + \nabla \mathbf{u}^T)$ is the strain-rate tensor.

The description of the molecular transport for multicomponent mixtures is a separate research discipline in itself and cannot be treated here in depth. Recent years have witnessed the publication of a large body of literature that builds on concepts from the kinetic theory of gases and aims at reducing uncertainties in transport coefficients, which can have important influences for flame extinction, ignition, and propagation, most particularly in the laminar regime where molecular transport is of paramount significance. The following could be considered a standard approach used for modeling transport in today's numerical codes for computational supersonic combustion. The heat flux is calculated from the expression $\mathbf{q} = -\lambda \nabla T + \sum_{i=1}^N \rho b_i Y_i \mathbf{V}_i$, where λ is the thermal conductivity. The Dufour effect is usually neglected as it tends to play a negligible role. Temperature-dependent heat capacities for relevant fuel–oxidizer mixtures and their combustion products are often obtained from an extensive database made available by McBride et al. (2005). The diffusion velocities \mathbf{V}_i , for instance, are calculated using the Curtiss–Hirschfelder approximation with a mass corrector, $\mathbf{V}_i Y_i = -W^{-1}(D_i W_i \nabla X_i - \sum_{k=1}^N D_k W_k Y_k \nabla X_k)$ (Giovangigli 1991), where X_i is the molar fraction and D_i is the diffusion coefficient of species i into the mixture. In H₂-air combustion, it is convenient to use more elaborate expressions of \mathbf{V}_i that account for thermal diffusion, by which light species such as H₂ and H tend to drift toward hot zones (Sánchez & Williams 2014). The dynamic viscosity μ of the mixture generally depends on temperature and can be obtained from Wilke's mixing rule based on the individual viscosities calculated from collision parameters (Hirschfelder et al. 1954). The most straightforward way of computing the thermal conductivity λ and D_i is by presetting constant values of Prandtl and Lewis numbers, respectively. Conversely, more elaborate results from the kinetic theory can be used to obtain these coefficients from first principles (Kee et al. 1986, Middha et al. 2002).

3.1.2. Flight corridor and combustor entrance conditions. The flight corridor of a scramjet-powered vehicle is in the stratosphere at 20–30-km altitude and $Ma_\infty = 6$ –10 cruise speeds (**Figures 2a** and **4b**). Lower altitudes cause excessive drag and aeroheating. Conversely, higher altitudes lead to oxidizer starvation and higher ambient entropy, which is tantamount to increasingly less energy available to be converted into thrust. Similarly, as the flight speed decreases outside this corridor, the flow becomes subsonic in the engine due to the deceleration caused by shock trains, and transition to ramjet mode is warranted if dual-mode operation is supported.

Conversely, the thrust-to-drag ratio and the specific impulse of scramjets decrease as the flight speed increases because the heat released by combustion becomes an increasingly smaller fraction of the air kinetic energy. As a result, at speeds above Mach \sim 10, scramjets typically provide smaller velocity increments per unit mass flow of propellant than other classic propulsion systems such as rocket engines.

The characteristic thermodynamic conditions of the undisturbed air environment within the flight corridor are $P_\infty \sim 0.01\text{--}0.05$ bar, $T_\infty \sim 215\text{--}230$ K, and $T_{0,\infty} \sim 1,800\text{--}4,800$ K, the last of which indicates a stagnation value. The conditions at the combustor entrance depend on the particular design of the forebody and inlet compression ramps, because they are determined by the spatial arrangement of the shocks. Characteristic overall deflection angles of the air streamlines of order $20\text{--}35^\circ$, to be split into three to four oblique shock waves, yield approximate ranges $P_A \sim 0.5\text{--}5$ bar, $T_A \sim 800\text{--}1,400$ K, and $Ma_A \sim 2\text{--}4$ for the combustor entrance conditions in the flight corridor, which are similar to those used in the configurations in **Figure 5**. Although the flight speeds are in the hypersonic range, the air velocities and Mach numbers in the combustor are approximately a factor of 2–3 smaller due to flow decelerations caused by interactions with shock waves across the forebody and inlet.

Forebody lengths of order 15–20 m in conceptual full-size hypersonic aircrafts, such as SR-72 or NASP, are sufficiently long to warrant a natural transition to turbulence in the boundary layers ingested in the scramjet engine. However, as the total length of the vehicle decreases to 3–5 m, as in hypersonic cruise missiles or unmanned aircrafts (**Figures 3** and **4b**), and as the velocity and altitude become closer to their lower and upper bounds in the flight corridor, respectively, the transition region is delayed and may penetrate into the engine, thereby leading to undesirable performance including inlet unstart and localized thermomechanical loading. As a result, boundary-layer trips have been employed in the forebody surfaces of HIFiRE-2 and X-43A to avoid these issues (Berry et al. 2010). Predicting transition in realistic flight conditions, including boundary-layer receptivity to high-altitude atmospheric disturbances, continues to be an important problem in hypersonics.

3.1.3. Supersonic combustion fuels. Most scramjet configurations are fueled with H_2 (e.g., X-43A, HIFiRE-3, HyShot-2, SCRAMSPACE, UVa configurations A–C, DLR, Stanford HTGL, ONERA/JAXA), JP-7 (e.g., X-51A), C_2H_4 (e.g., UVa configuration E), and mixtures of C_2H_4 with CH_4 (e.g., HIFiRE-2). In addition to these, silanes (SiH_4) have been used in X-43A flights as an additive to facilitate ignition because of their high reactivity with oxygen (McClinton 2006). In many cases, the gaseous fuels are injected at near-sonic conditions at ambient temperature, translating to fuel stream velocities of order 1,440 m/s for H_2 and 340 m/s for C_2H_4 . Correspondingly, the characteristic Reynolds numbers of the fuel jets are $Re_d \sim 10^4\text{--}10^5$ based on typical injector orifice diameters $d \sim 1\text{--}3$ mm.

Hydrogen has a large energy density, leading to specific impulses higher than other fuels, and can be cryogenically stored to reduce volume. Conversely, C_2H_4 has less energy density but can be stored in liquified form by pressurizing it at ambient temperature without the need of cryogenic systems. Binary 64% C_2H_4 /36% CH_4 mixtures behave as fuel surrogates with combustion characteristics similar to cracked JP-7 (Pellet et al. 2008). Originally developed for the SR-71, JP-7 has an energy density comparable to that of C_2H_4 but is thermally stable with an initial endothermic decomposition stage that makes it attractive as a heat sink for the regenerative cooling of the scramjet walls. Unless prevaporized, JP-7 is in liquid state at injection and has to be atomized and vaporized by the supersonic air coflow, which is a difficult problem that has nonetheless witnessed progress (Mathur et al. 2000). Ethylene has also been used in the X-51A for ignition and for preheating the JP-7 flowing in the wall cooling channels. The development of chemical-kinetic models for complex hydrocarbon fuels for supersonic combustion is an active research topic that

has recently revealed some important modeling simplifications to decouple the fuel pyrolysis stage from the oxidation of fuel decomposition intermediates using hybrid chemistry (Xu et al. 2017).

The combustor entrance conditions described in Section 3.1.2 are relevant for addressing the performance of these fuels. For instance, it is known that some aspects of hydrogen kinetics such as autoignition in high-speed coflows of the type sketched in **Figure 7a** are highly sensitive to whether the temperature of the air stream is above or below the crossover value T_c ($T_c \sim 900, 950$, and $1,000$ K at $P = 0.5, 1$, and 5 bar, respectively). Specifically, T_c is defined as the temperature at which the rates of production and consumption of H radicals become equal, $k_2[M] = 2k_1$, where $[M]$ is the molar concentration of the collider and k_1 and k_2 are the rates of the reactions $\text{H} + \text{O}_2 \xrightarrow{1} \text{OH} + \text{O}$ and $\text{H} + \text{O}_2 + \text{M} \xrightarrow{2} \text{HO}_2 + \text{M}$, respectively.

For $T_A > T_c$, the ignition process begins with a slow production of radicals from collisions between H_2 and O_2 through the main initiation reaction $\text{H}_2 + \text{O}_2 \xrightarrow{3} \text{HO}_2 + \text{H}$. This stage can be easily bypassed by small initial concentrations of radicals produced by lasers or plasmas (Brieschenk et al. 2013, Ju & Sun 2015), O_2 dissociation (Da Riva & Urrutia 1968), or facility impurities (Urzay et al. 2014) including air vitiation used in scramjet ground-based tests (Goyne et al. 2007). When the concentration of radicals generated by step 3 is sufficiently large, a rapid branched-chain explosion follows whereby the concentration of the radical pool increases exponentially near the air boundary in a thermally frozen field to leading order. The computations can be simplified by a five-step mechanism (Del Álamo et al. 2004), yielding ignition times of order $t_{ig} \sim t_B \ln(\epsilon^{-1}) = 20\text{--}50 \mu\text{s}$ for $P \sim 1$ bar and $T_A \sim 1,200\text{--}1,400$ K, where t_B is the minimum branching time in the mixing layer and $\epsilon = k_3/2k_1 = \mathcal{O}(10^{-7})$ is a characteristic branching-to-initiation time evaluated at that minimum (Sánchez & Williams 2014). These simplified estimates compare well against Cheng et al.'s (1994) measurements and do not differ significantly from the homogeneous ignition times based on T_A shown in **Figure 8a**. The corresponding ignition distances are of order $L_{ig} \sim U_A t_{ig} \sim 30\text{--}125$ mm for airflow velocities $U_A \sim 1,500\text{--}2,500$ m/s in the $Ma_A \sim 2\text{--}4$ range of combustor entrance conditions, but they become rapidly inadmissible from a practical standpoint as the temperature decreases below 1,200 K because they involve the entire or significant fractions

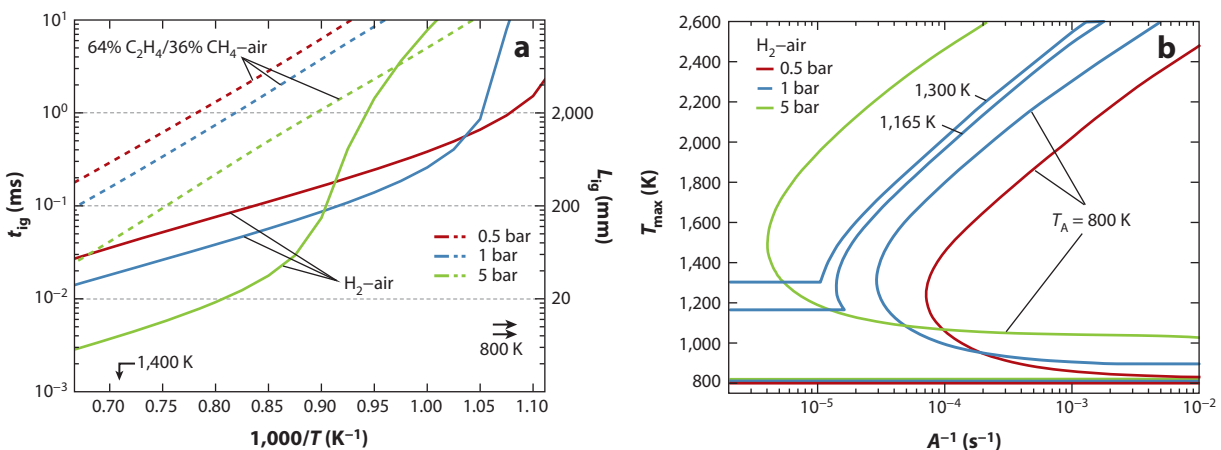


Figure 8

(a) Homogeneous ignition times for stoichiometric mixtures of H_2 and $64\% \text{C}_2\text{H}_4/36\% \text{CH}_4$ with air in the flight corridor, including characteristic ignition lengths for a convective velocity of $2,000$ m/s. (b) H_2 -air counterflow laminar diffusion-flame curves for $T_F = 300$ K. The mechanisms used are Stanford for H_2 (Hong et al. 2011) and USC-II for $\text{C}_2\text{H}_4/\text{CH}_4$ mixtures (Wang et al. 2007).

of the scramjet combustor length (i.e., 300 mm in HyShot-2, 225 mm in UVa's, 200 mm in DLR's; see **Figure 5**). Below crossover, ignition occurs through reactions involving H_2O_2 in times of order 1 s or larger, leading to exceedingly long ignition distances. For H_2 -air supersonic combustion, the low-temperature range of the combustor entrance conditions, which is most likely encountered as the flight speed decreases and in scramjets with short or no isolators, must involve flame stabilization methods other than lifted autoignition, as discussed in Section 3.1.4. The situation worsens for JP-7 or its surrogate 64% C_2H_4 /36% CH_4 , both of which involve additional chemical stages and render ignition times comparable to or longer than flow residence times in standard configurations across the entire temperature range of the flight corridor.

Although the S-shaped curve in the analysis of counterflow diffusion flames by Liñán (1974) was limited to single-step kinetics, the qualitative dynamics tend to persist even when complex chemistry is included. However, there are some exceptions that are worth mentioning with regard to the multivalued character of the curves, particularly if flamelet-based turbulent supersonic combustion modeling for H_2 -air flames is pursued (see Section 3.2.1). In particular, the solution is highly dependent on the air temperature in the case of H_2 -air diffusion flames (Sánchez et al. 1996), as shown in **Figure 8b**. Specifically, for $T_{\text{A}} < T_{\text{c}}$, the chain-termination step 2 is too fast and prevents the development of branched-chain ignition. As a result, the lower turning point involves asymptotically large straining times. Conversely, for $T_{\text{c}} < T_{\text{A}} \lesssim T_{\text{c}} + 200$ K, the curve resembles the traditional S-shaped one yielding multiple values for a single strain rate. However, for $T_{\text{A}} \gtrsim T_{\text{c}} + 200$ K, the curve becomes single valued in the strain rate and shows no abrupt extinction or ignition phenomena. The latter corresponds to the relevant regime in the HyShot-2 scramjet configuration (Urzay et al. 2012).

3.1.4. Shock-induced combustion. A complex system of shocks and expansion waves develops in the scramjet in a manner that is strongly influenced by the forebody, inlet, combustor geometry, and the fuel-injection configuration (**Figure 7d**). The order-unity variations in P and T associated with such a system can be harvested to ignite mixtures that would otherwise remain chemically frozen. Such a phenomenon has been termed shock-induced combustion (Rubins & Bauer 1994), is closely related to mixing enhancement in some cases, and can occur in different configurations, as in the few examples in **Figure 9**. A subdivision of shock-induced combustion can be performed by distinguishing whether the reactants in the shocked gas are premixed or nonpremixed.

The premixed mode of shock-induced combustion so far has had its most prominent application not in scramjets but in shock tubes to measure kinetic rates and ignition times, where the involved physics serve to illustrate some of the important aspects of this problem. There, a driver section is filled with an inert high-pressure gas separated by a diaphragm from a driven test mixture whose initial thermodynamic conditions are sufficiently mild to prevent autoignition. When the diaphragm is relieved, a mostly planar shock propagates into the driven mixture in such a way that the incident or reflected passage of the shock leaves the mixture at higher pressure and temperature. Ignition occurs after a time delay in a zone that is physically separated from the moving shock when the pressures and shock speeds are moderate. As in many other problems related to shock-induced combustion described below, the disturbance created by the shock is sufficiently fast that molecular transport plays a negligible role in the ignition process (Jackson & Kapila 1985). This represents an important characteristic that fundamentally separates shock-induced combustion from the diffusion-controlled combustion problems discussed in the context of **Figure 7a–c** and that poses a different paradigm in the SGS modeling of these phenomena.

A process with characteristics similar to premixed shock-induced combustion has been tested in the HIFIRE-3 and SCRAMSPACE scramjets and requires geometries relatively simpler than other configurations where flameholders are necessary. In these engines, hydrogen is injected

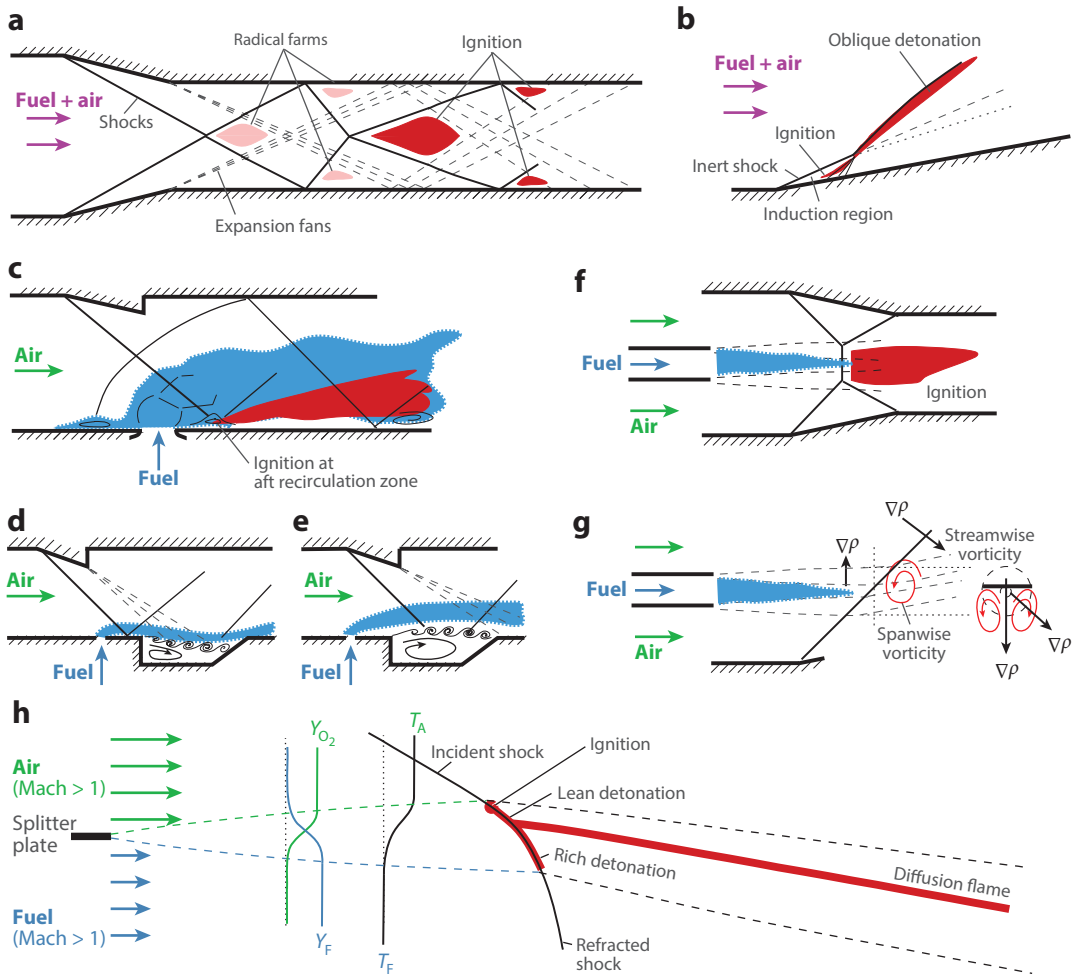


Figure 9

Schematics of shock-induced mixing and combustion problems: (a) radical farming, (b) oblique detonation wave, (c) near-wall shock-induced combustion, (d) shock-on-jet and (e) shock-on-cavity impingement effects on shear layers in cavity-based scramjet combustors, (f) normal-shock-induced ignition of a fuel jet, (g) oblique-shock-induced mixing in a fuel jet, and (h) diffusion-flame ignition by shock impingement on a supersonic mixing layer.

in crossflow at the inlet and mixes with the ingested air, whose temperature is below crossover, preventing ignition there. The gases arrive in a mostly premixed state at the combustor, where their temperature and pressure are increased by shocks and decreased by expansion waves. In particular, flow islands bounded upstream by shocks and downstream by expansion waves attain near-crossover temperatures that serve as radical farms where small but finite amounts of radicals are produced and accumulate (**Figure 9a**). According to simulations and experiments by Odum & Paull (2007), McGuire et al. (2008), and Lorrain et al. (2012), shock-induced combustion occurs in these systems as a cumulative multistage process by which radicals produced in the farms are convected to other farms, where the reshocked gas temperature increase favors further radical buildup that eventually leads to hot spots where the chain is terminated and heat is released.

At higher pressures or inflow velocities, the ignition time in the premixed gases decreases and closer interaction between the reaction zone and the shock wave is attained in the form of a detonation, which corresponds to a supersonic reacting wave that leaves burnt gases behind at elevated pressure, density, and temperature. In particular, stabilized oblique detonation waves have been under consideration for scramjets, where fuel and air are premixed at the inlet, because they serve to steadily burn the incoming mixture while leaving it supersonically behind (Pratt et al. 1991). In these scramjets, the premixed gases are flown over a compression ramp located at the combustor entrance, which generates an oblique shock emanating from the corner (**Figure 9b**). At flow velocities larger than the Chapman–Jouguet detonation speed and moderately high streamline deflection angles, the reaction zone couples acoustically with the oblique shock and forms a standing detonation wave stabilized at the corner. The resulting structure consists of an oblique detonation wave away from the wall, along with an inert portion of the shock near the corner trailed by an induction zone that gives rise to an ignition front (Li et al. 1994, Morris et al. 1998).

The nonpremixed mode of shock-induced combustion is relevant for most scramjet configurations, in which the fuel is injected directly into the combustor rather than the inlet. In these systems, shock waves ubiquitously interact with mixing regions, where combustion chemical reactions are bound to occur. In principle, the dominant effect of incident shocks on such regions consists of locally increasing pressure and temperature, thereby providing favorable thermodynamic conditions for ignition. However, shocks modify the mixing between reactants by introducing additional vorticity and perturbing near-wall flame stabilization regions by interacting with sidewall boundary layers.

In some configurations, the region of interest for shock-induced combustion is near the combustor wall where the flow is much slower than the free stream. For instance, in jet-in-crossflow scramjets such as HyShot-2 (**Figure 5b**), adverse pressure gradients associated with the transverse injection cause near-wall recirculation zones where fuel mixes with air near the fore stagnation point and in the wake of the jet. In a similar configuration, Gamba & Mungal (2015) observed that these zones play an important role in providing a mechanism for flame anchoring due to the increased residence times there (**Figure 6b**). In particular, the aft recirculation zone of the jet can be strengthened by the additional adverse pressure gradient caused by the impingement of an oblique shock created by a wedge on the opposite wall (**Figure 9c**). This aerodynamic effect was recently used by Mai et al. (2011) as a method for shock-induced ignition.

Similar phenomena have been studied in HIFiRE-2 (**Figure 5a**), in which flame stabilization largely relies on the long residence times in the side cavities where the flow is predominantly subsonic, as Barnes & Seagal (2015) described in detail in their recent review dedicated to cavity flameholders. Depending on the operating parameters, flame stabilization may occur near the wall in the wake of the primary fuel injectors, in the overriding shear layer formed between the cavity gases and the free stream, or as a combination of both modes (Micka & Driscoll 2009). There has been recent interest in analyzing the effects of shock trains created by the specific geometries of the forebody and inlet of HIFiRE-2 under different angles of attack, which are not easily reproduced on the ground in direct-connect rigs for ground-based experiments, where only the combustor is tested while connected to a supersonic nozzle. In real flight, the shock train may penetrate into the combustor, generating flow distortions and unexpected shock-induced mixing and combustion. Specifically, the impingement of shock waves on either the primary fuel jet or the cavity shear layer has distinct consequences on mixing, combustion, and forced ignition, as Etheridge et al. (2012), Kirik et al. (2014), and Ombrello et al. (2015) have shown. Whereas the former pushes the shear layer deeper into the cavity and results in a higher concentration of fuel there (**Figure 9d**), the latter lifts the shear layer above the cavity and stretches the fuel plume in the spanwise direction (**Figure 9e**). Both mechanisms are related to expansion waves (in the former) and shock waves (in

the latter) imposing pressure variations along the shear layer, which are elliptically transmitted to the subsonic flow in the cavity and have to be compensated by streamline curvature on the supersonic side.

The ignition distance of hydrogen jets parallel to supersonic air coflows can be shortened by using oblique and Mach-reflected normal-shock systems created by single or double wedges (Rhodes et al. 1962), as schematically shown in **Figure 9f**. The oblique case (**Figure 9g**) leads to the augmentation of mixing by baroclinic vorticity introduced by the misalignment between the shock pressure gradient and the density gradient across the mixing layer (Marble 1994, Hermanson & Categen 2000).

The interaction of oblique shocks with mixing layers is a phenomenon experimentally observed in the DLR scramjet. There, the shock created by the wedge reflects on the sidewall, crosses both the expansion fan generated at the wedge-trailing corner and the recompression shock emanating from the wake, and impinges on the mixing layer where it is reflected as an expansion wave (**Figure 7d**). The flow on the fuel side of the mixing layer near the wedge base becomes subsonic because of the heat released by combustion. The higher pressure of the postshock gases around the impingement point is transmitted upstream along the subsonic fuel side, which contributes to the vase-like shape of the reacting jet. Although ignition occurs in the recirculation region near the wedge base, planar laser-induced fluorescence (PLIF) visualizations reported by Waidmann et al. (1994) indicate that OH emissions are increased at the impingement point, thereby suggesting a shock-induced intensification of the diffusion flame.

In the laminar regime, the problem of a weak shock interacting with a transonic mixing layer at high Reynolds numbers is reminiscent of the classical weak-shock/boundary-layer interaction first studied by Lighthill (1950) and later by Stewartson & Williams (1969) using triple-deck theory, with the exception that here it is unnecessary to deal with the viscous low-speed near-wall deck. In the first approximation, the problem can be solved by considering the propagation of inviscid disturbances created by the weak shock in the self-similar mixing layer profiles near the impingement location, which give rise to a modified Prandtl–Glauert equation for the pressure waves that can be solved asymptotically using Fourier methods (Huete et al. 2016). The weak shock pressure disturbances are transmitted to the subsonic side up to streamwise distances of the same order as the thickness of the mixing layer at the impingement location, thereby setting a fundamental difference with respect to Lighthill’s weak-shock/boundary-layer problem, in which the pressure disturbances are propagated much farther along the wall from the impingement point. The interaction of the transonic mixing layer with finite-strength shocks, in which the local disturbance is significant as required for ignition, is however much more challenging to solve, in that the resulting ellipticity of the pressure field on the subsonic side in principle precludes a local description because the solution may require that specific boundary conditions and the geometrical details of the combustor be considered.

Conversely, the problem of an oblique shock impinging on a mixing layer separating two supersonic streams of fuel and oxidizer can be locally described as follows. The oblique shock deflects both streams and bends across the supersonic mixing layer because of the generally different speeds of sound of the reactants. The problem can be treated in the weakly reacting limit using boundary-layer theory, appropriate jump conditions across the incident shock, and the method of characteristics in the postshock gases with a Frank–Kamenetskii expansion of the exponential temperature dependence of the reaction rate based on small departures from the frozen temperature (Huete et al. 2015). The structure of the resulting ignition kernel is analytically described by the competition between heat release and acoustic waves from the trailing expansion fan that tend to decrease the temperature, as opposed to the competition between heat release and transverse molecular diffusion encountered in the nonpremixed ignition fronts analyzed by Liñán & Crespo

(1976). **Figure 9f** depicts a typical postignition scenario formed by a detonative front and a trailing diffusion flame for the case where the Mach number of the air stream is sufficiently small to prevent significant aerodynamic heating (Huete et al. 2015). Similar analyses have been recently extended to incorporate hydrogen-air chemistry (Huete et al. 2017). The impingement of oblique shock waves on nonreacting mixing layers in the turbulent regime, which corresponds to the most realistic one in practical applications, has been analyzed experimentally by Brummund & Nuding (1997) and numerically by Génin & Menon (2010b) using LES, although the reacting counterpart is a problem that largely remains to be understood at the fundamental level. The use of shock waves to control supersonic combustion in scramjets continues to be a challenging problem at the frontier in high-speed chemically reacting turbulent flows.

3.1.5. Compressibility effects on turbulent supersonic reacting mixing layers. For the reasons explained in Section 3.1.1, much of the research in supersonic combustion has focused on the structure of diffusion flames. Most of these studies have unraveled complex chemical-kinetic effects in canonical problems such as counterflow laminar diffusion flames, which are pivotal for modeling turbulent nonpremixed combustion (**Figure 7b,c**). Advanced experimental diagnostics and numerical solvers that can rapidly integrate the 2D self-similar conservation equations subject to stiff chemical reaction terms have been the primary tools to study these flows. However, diffusion flames in scramjet engines are almost always embedded in turbulent supersonic mixing layers, which complicates the description.

To illustrate, consider the turbulent mixing layer sketched in **Figure 7b**. At high Mach numbers, compressibility effects that are related to acoustic radiation and vortex pairing suppression tend to decrease the growth rate $d\delta_\theta/dx_1$ of the turbulent mixing layer, thereby precluding the entrainment of reactants and the subsequent molecular mixing necessary for chemical reactions to develop. A parameter that quantifies the importance of compressibility effects of the relative turbulent motion between the fuel and air streams is the convective Mach number, $Ma_C = (U_A - U_C)/a_A$, where $U_C = (U_A a_F + U_F a_A)/(a_A + a_F)$ is the convective velocity when the adiabatic coefficients of fuel and air are not too different, with a_F and a_A the sound speeds in the fuel and air streams, respectively. In particular, the suppression of the growth rate starts becoming noticeable at $Ma_C \sim 0.4$ and plunges to 30% of its incompressible value at $Ma_C \sim 1$ (Papamoschou & Roshko 1988). Chemical heat release further inhibits the growth rate due to a decrease in the Reynolds shear stresses caused by a decrease in density (Hermanson & Dimotakis 1989). The characteristic values of the convective Mach number in scramjet combustors range from 0.8 for hydrogen and 2.3 for ethylene near the fuel injector ($Ma_A \sim 4$, $T_A \sim 1,300$ K, $Ma_F \sim 0.5$, and $T_F \sim 500$ K) to 1.4 for hydrogen and 0.2 for ethylene far from the fuel injector where supersonic diffusive combustion has been established ($Ma_A \sim 2$, $T_A \sim 1,300$ K, $Ma_F \sim 2$, and $T_F \sim 2,000$ K). This illustrates the variabilities in Ma_C that can be encountered depending on the fuel properties and the spatial location in the combustor.

Besides influencing integral quantities, the high Mach numbers encountered in supersonic combustion applications also involve localized effects in the form of a multitude of small shocks and expansion waves acoustically generated within the mixing layer as a result of the compressible turbulent relative motion between both streams. These effects have been much less studied, particularly in chemically reacting mixing layers, because they are difficult to quantify computationally or experimentally due to the high spatiotemporal resolution required. In the context of supersonic combustion, direct numerical simulations (DNS) have been useful in understanding these phenomena (Mahle et al. 2007, Ferrer et al. 2017), although the problem remains an active topic of research. One simplified way of studying it, which does not require the costly simulation of the entire spatial development of the mixing layer, is by DNS in a reference frame moving at the mean velocity $U_m = (U_A + U_F)/2$ such that the problem reduces to two supersonic free streams flowing

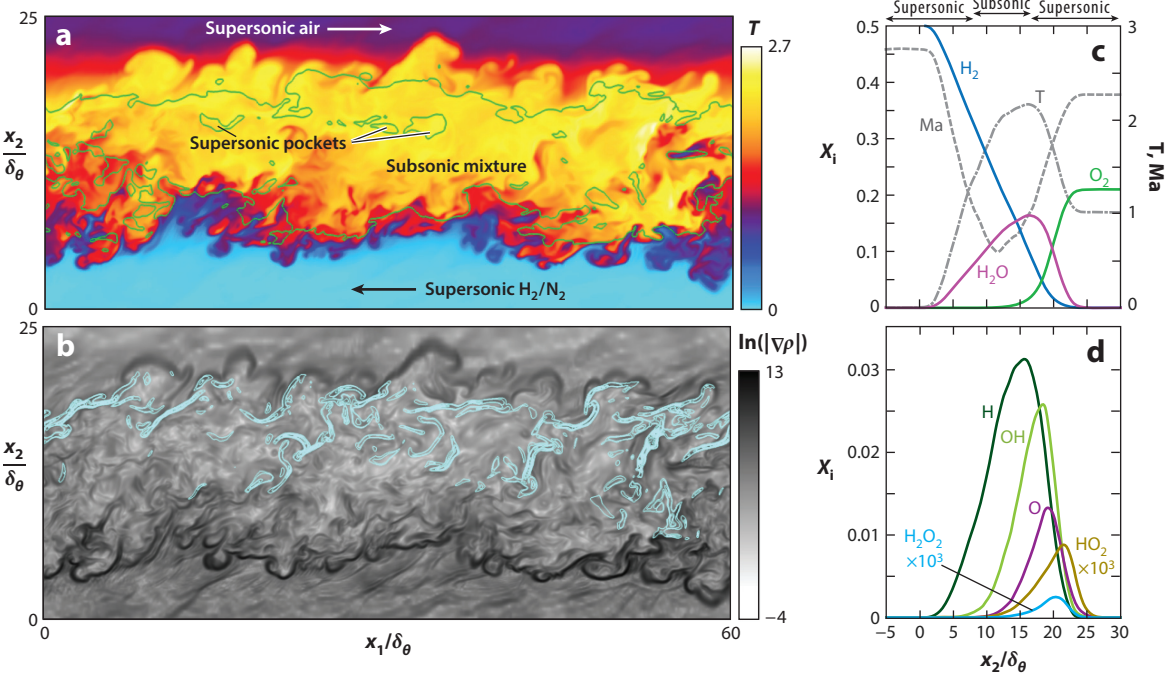


Figure 10

Three-dimensional direct numerical simulation of a hydrogen-fueled reacting turbulent supersonic mixing layer. (a) Streamwise mid-plane contours of the static temperature T redefined in dimensionless form as $(T - T_F)/(T_A - T_F)$, including upper and lower sonic lines (green). (b) Solid contours of the static density gradient modulus $|\nabla\rho|$ normalized with $(\rho_F - \rho_A)/\delta_\theta$, including isolines of the H-radical production rate ($0.1 < i_H/i_{H,\max} < 1.0$) (cyan). Panels c and d provide planar-averaged profiles across the mixing layer for static temperature, local Mach number $Ma = |\mathbf{u}|/\sqrt{\gamma R_g T}$, with γ the local adiabatic coefficient, along with molar fractions of main and minor species.

in opposite directions at the same velocity $U = |U_A - U_F|/2$ in a streamwise-periodic domain, with the corresponding convective Mach number given by $Ma_C = 2U/(a_A + a_F)$. An example of a DNS of such a configuration is provided in **Figure 10**, which corresponds to a 3D mixing layer separating air at Mach number $Ma_A = U/a_A = 2.25$ and $T_A = 1,500$ K from diluted hydrogen at $Ma_F = U/a_F = 2.73$ and $T_F = 500$ K in an ambient at $P = 2$ bar, which renders a convective Mach number of 2.47. The simulations integrate the formulation described in Section 3.1.1 with variable heat capacities and constant nonunity Lewis numbers, supplemented with the detailed H_2 -air mechanism by Hong et al. (2011), and without the Soret effect. Details are provided by O'Brien et al. (2014) and Saghafian (2014).

In turbulent mixing layers at high Mach numbers, the acoustic time δ_θ/a_A is of the same order as the characteristic large-scale eddy-straining time δ_θ/U , with associated localized variations of the thermodynamic pressure comparable to $\rho_A U^2$, the latter having important implications for turbulent combustion modeling as described in Section 3.2. As the two streams are entrained in the mixing layer, they encounter regions of decreasing velocity and eventually become subsonic in the relative reference frame, as indicated in **Figure 10a** by the sonic lines delimiting the central subsonic portion of the mixing layer. There, the free-stream kinetic energy is partially recovered as thermal energy, causing a large increase in temperature proportional to the square of the Mach number of the relative motion. This temperature increment can be significant even in nonreacting

cases and can elevate combustion temperatures above those expected for subsonic mixing layers under the same strain rate. The flow deceleration may take place abruptly between adjacent eddies carrying supersonic and subsonic flows, generating thin compression regions where order-unity variations in P , T , ρ , and Mach number occur that are statistically manifested as high spatial intermittency in the flow dilatation. These regions have been traditionally termed eddy shocklets (Zeman 1990, Lee et al. 1991, Miller et al. 1994) and are reminiscent of small-scale structures observed within the mixing layer near the fuel side in **Figure 10b**.

Despite this welter of additional complexities in high-Mach number flows, the high temperatures caused by the combustion heat release tend to suppress compressibility effects on turbulence by effectively decreasing the local Mach number. As a result, in the example given above, the chemical reactions tend to develop for a good part within the subsonic region of the mixing layer, although significant exceptions are found in the internal supersonic pockets and in the supersonic flow near the air side (**Figure 10c,d**). Nonetheless, these remarks only pertain to compressibility effects on the turbulent relative motion between the two streams because combustion chemical reactions may still occur abundantly at supersonic flow velocities in the laboratory frame. This is observed, for instance, away from walls in jet-in-crossflow scramjet combustors, where diffusion flames burn in supersonic regions enveloping the fuel jet (see **Figure 6b** and Section 3.2.3). Further research on these aspects is warranted, including investigations of the influences of shocklets on the production of reaction intermediates. To this end, systematic detection algorithms of shocklets using physics-based thresholds and computer imaging may be useful, as done, for instance, by Samtaney et al. (2001).

3.2. Large-Eddy Simulation of Scramjets

The advent of LES in solving multiphysics turbulent flows has recently enabled the investigation of complex supersonic combustion phenomena in scramjets that were not accessible before with Reynolds-averaged Navier–Stokes (RANS) models or purely theoretical methods. This section focuses on SGS modeling and full-system LES, including the computation of scramjet unstart.

3.2.1. Turbulent supersonic combustion modeling. LES is based on resolving the flow scales larger than the grid cutoff Δ_{LES} while modeling the subgrid scales. As indicated in Section 3.1.1, the diffusion-controlled regime of combustion prevails in scramjet combustors away from walls, flameholders, and fuel injectors. In this regime, turbulent mixing layers such as the one in **Figure 10** separate the fuel and oxidizer streams. Both reactants are entrained in the mixing layer by the engulfing motion of large eddies of the same size as the mixing-layer thickness. Eddies cascade down into smaller eddies until the Kolmogorov scale ℓ_k is reached (or a multiple of it for preferentially diffusing scalars), where molecular diffusion enables the fine-grained mixing of reactants and the subsequent development of combustion chemical reactions in thin reacting layers, which have a thickness δ_f and are subject to a characteristic strain rate of order $A \sim v/\ell_k^2$ (**Figure 7b**). Ascribing the idealized, single-step, low-Mach laminar flame structure of Liñán (1974) to the reaction layers embedded in the Kolmogorov eddies, their thickness δ_f is smaller than ℓ_k by a factor of order $\Delta_0^{-1/3}/\beta$, where $\Delta_0 \sim (\chi_{\text{st}} t_{\text{ch,f}})^{-1}$ is a local Damköhler number based on the flame chemical time $t_{\text{ch,f}} \sim (BY_{\text{O}_2,\text{A}} e^{-T_a/T_f} / \beta^3)^{-1}$ and on the stoichiometric scalar dissipation rate $\chi_{\text{st}} \sim AZ_{\text{st}}^2$. In the formulation, $Z_{\text{st}} \ll 1$ is the stoichiometric mixture fraction, and $\beta = T_a(T_f - T_a)/T_f^2 \sim 5-10$ is a Zel'dovich number proportional to the dimensionless activation temperature. Similar estimates may be made for H₂-air flames, where $t_{\text{ch,f}} \sim (k_2[\text{O}_2][\text{M}])^{-1}$ is associated with a heat-release time, β is approximated as $T_{\text{a}}(T_f - T_{\text{a}})/T_f^2$ based on the activation temperature of the main branching step 1, and Z_{st} is equal to 0.028 for undiluted H₂ streams.

More often than not, the turbulence intensity in the combustor is such that $\Delta_0 \gg 1$. Additionally, constraints on computational cost usually impose a grid spacing Δ_{LES} much larger than ℓ_k . As a result, Δ_{LES} is also much larger than the flame thickness δ_f by a factor of order $\Delta_{LES}/\delta_f \sim \beta \Delta_0^{1/3} (\Delta_{LES}/\ell_k) \gg 1$, with SGS modeling required for the chemical source term \bar{w}_i in the filtered version of Equation 4. Several options exist for SGS modeling of \bar{w}_i in the context of supersonic combustion. These have been reviewed extensively by Fureby (2012) and Gonzalez-Juez et al. (2017) and are not treated in depth here. The approaches range from neglecting the SGS contributions (Fulton et al. 2012) to using local partially stirred reactors (Chapuis et al. 2013), probability density function (PDF) methods (Koo et al. 2011), linear eddy models (Génin et al. 2003), and flamelets (Larsson et al. 2015). Although all require a number of approximations and might be similarly qualified, the last of these is the one that can be most straightforwardly associated with a physical representation of turbulent diffusion flames and is therefore the subject of some remarks below motivated by recent investigations regarding its use for supersonic combustion.

In the standard, steady nonpremixed flamelet model (Peters 2000), the filtered versions of the mass and momentum conservation Equations 1 and 2 are solved along with two additional transport equations: one for the resolved mixture fraction \tilde{Z} , which is a sourceless advection-diffusion equation with a molecular diffusivity that in practice is taken to be equal to the thermal diffusivity, and another one for its SGS variance \tilde{Z}''^2 , which is often substituted by a dynamic model for \tilde{Z}''^2 based on the gradients of \tilde{Z} (Pierce & Moin 1998). In addition, a microscale model problem consisting of a low-Mach, steady counterflow laminar diffusion flame is solved in Z space subject to Dirichlet boundary conditions for T and Y_i , corresponding to the values of temperature and composition, respectively, of the fuel and air streams at their conditions of injection in the combustor. This integration provides solutions of the form $Y_i(Z, \chi_{st})$ and $T(Z, \chi_{st})$, where χ_{st} plays the role of a sweeping parameter that is related to the resolved strain rate A through a modeled expression of exponential error function type that dates back to Liñán (1974). The corresponding filtered values are $\{\tilde{Y}_i, \tilde{T}\} = \int \{Y_i, T\} \tilde{P}(Z, \chi_{st}) dZ d\chi_{st}$, where $\tilde{P}(Z, \chi_{st})$ is a joint PDF that represents SGS mixing and straining processes not captured in LES and depends on the local values \tilde{Z} , \tilde{Z}''^2 , and $\tilde{\chi}_{st}$ obtained by solving the LES transport equations. In this way, the pretabulated solutions of the microscale problem provide $\tilde{Y}_i(\tilde{Z}, \tilde{Z}''^2, \tilde{\chi}_{st})$ and $\tilde{T}(\tilde{Z}, \tilde{Z}''^2, \tilde{\chi}_{st})$ on the fly.

At least five important problems arise when this model is applied to compute turbulent supersonic combustion in scramjets, which have inspired several improvements in recent years. The first problem pertains to upgrades required when the response of the microscale problem involves a multivalued S-shaped curve (**Figures 7b** and **8b**), which cannot be reproduced in its entirety by using χ_{st} as the sole sweeping parameter. To enable access of the steady nonpremixed flamelets to the lower branch and the ignition point and to provide a model for ignition in partially premixed zones near the fuel injector, Pierce & Moin (2004) proposed a single-valued remapping of the solution in the flamelet progress variable approach (FPVA) in terms of a progress variable C , which represents the degree of completion of the combustion process (e.g., $C = Y_{H_2O}$ in H₂-air systems). Generalizations of this model are available to support premixed combustion modes (Knudsen & Pitsch 2009). In the FPVA model, an additional LES transport equation for C is solved that contains a filtered chemical source \bar{w}_C closed with the model. The filtered values of mass fractions, temperature, and progress variable source become $\{\tilde{Y}_i, \tilde{T}\} = \int \{Y_i, T\} \tilde{P}(Z, C) dZ dC$ and $\bar{w}_C = \int \dot{w}_C(Z, C) \tilde{P}(Z, C) dZ dC$, where $\tilde{P}(Z, C)$ and $\tilde{P}(Z, C)$ are density-weighted and unweighted joint PDFs modeled using beta and delta functions that depend on \tilde{Z} , \tilde{Z}''^2 , and \tilde{C} . By integrating the LES transport equations, one obtains the local values of \tilde{Z} , \tilde{Z}''^2 , and \tilde{C} to use in reading the pretabulated solutions of the microscale problem to provide $\tilde{Y}_i(\tilde{Z}, \tilde{Z}''^2, \tilde{C})$, $\tilde{T}(\tilde{Z}, \tilde{Z}''^2, \tilde{C})$,

and $\bar{w}_C(\tilde{Z}, \widetilde{Z''^2}, \tilde{C})$ on the fly. However, as described in Section 3.1.1, the ignition point in the S curve is not indicative of autoignition in the evolution type of flows found in scramjets, in which two streams of fuel and oxidizer mix together and ignite either by shock induction or when sufficiently high temperatures have enabled the decomposition of fuel molecules into enough radicals in the mixing layer. These processes require that one consider the parabolic time histories as opposed to the elliptic, boundary-value formulation that leads to the S curve. Modifications have been proposed in the microscale problem to target unsteady effects (Mellado et al. 2000) and address autoignition processes using unsteady versions of the FPVA model (Ihme & See 2011).

The second problem involves the computation of the resolved temperature \tilde{T} . At low Mach numbers, the background pressure is mostly uniform, and the density becomes a sole function of Y_i and T , both of which can be obtained from the flamelet table. Conversely, at high Mach numbers, it becomes necessary to integrate the filtered version of the total energy Equation 4, leading to discrepancies between the temperature \tilde{T} computed from that equation and the temperature \tilde{T}_{tab} obtained from the flamelet table. These differences are caused by the exchanges between kinetic and thermal energy described in Section 3.1.5. Pecnik et al. (2012) proposed a method of reconciliation between the flamelet and LES temperatures in the FPVA model that results in the simple expression $\tilde{T} \simeq \tilde{T}_{\text{tab}} + (\tilde{\gamma}_{\text{tab}} - 1)\alpha_{\tilde{\gamma},\text{tab}}^{-1}\{\exp[\alpha_{\tilde{\gamma},\text{tab}}(\tilde{e} - \tilde{e}_{\text{tab}})/\tilde{R}_{g,\text{tab}}] - 1\}$ in terms of the internal energy e and the adiabatic coefficient variations $\alpha_{\gamma} = dy/dT$. This relation enables an approximate but straightforward computation of the resolved temperature \tilde{T} given \tilde{e} and the three tabulated variables \tilde{Z} , $\widetilde{Z''^2}$, and \tilde{C} without the need for expensive numerical iterations at every time step.

The third problem corresponds to the compressibility effects that are significant in high-Mach turbulent flows, as described in Section 3.1.5, but are absent in the microscale problem solved in the flamelet model. The low-Mach laminar counterflow is conceptually deficient as an abstraction of the small scales of compressible turbulence bearing intermittent flow dilatation, order-unity variations of the thermodynamic variables, and dilational dissipation caused by shocklets. Nevertheless, recent studies have focused on incorporating in the FPVA model some of the effects of the local variations of pressure and temperature caused by resolved compressibility phenomena in scramjets. Instead of adding \bar{P} and \tilde{T} as costly dimensions in the flamelet table, simpler approaches have had success by correcting the progress variable source term either with a model power-like dependence on the resolved density along with an exponential temperature correction, $\bar{w}_C/\bar{w}_{C,\text{tab}} \simeq (\bar{\rho}/\bar{\rho}_{\text{tab}})^{\eta_{\text{tab}}} \exp[-T_a(1/\tilde{T} - 1/\tilde{T}_{\text{tab}})]$ (Saghafian et al. 2015b), or by using a first-order expansion of \bar{w}_C in \bar{P} and \tilde{T} around the flamelet table values (Shan et al. 2017).

The fourth and fifth problems pertain to specific aspects of near-wall burning and multifuel fueling systems in scramjet engines, respectively. The significant amount of near-wall burning observed in supersonic combustion experiments (**Figure 6b**) is important for the stabilization of flames in the fore and aft recirculation regions near the injection orifices of fuel jets in crossflows. Since in most practical situations the near-wall region is poorly resolved, incorporating this phenomenon into LES most likely requires augmenting wall models, rather than using flamelets, to account for flames in boundary layers. Similarly, a framework of multiple mixture fractions for flamelets is required in multistage fuel-injection systems (Doran 2011), whose different ports may provide different fuels or the same fuels at different thermodynamic conditions, depending on the flight parameters.

3.2.2. Full-system simulations. LES constitutes a modern revolution in the analysis of full scramjet engines. Although its widespread use in hypersonic propulsion technology is still in its infancy, its potential for simulating supersonic combustion in complex geometries is evident.

However, full-system LES of scramjets face the following set of computational grand challenges that are active topics of research: (*a*) physics-based turbulent supersonic combustion modeling, including multiregime flame structures and the appropriate characterization of the chemical kinetics of complex fuels; (*b*) low-dissipative numerical methodologies for highly compressible turbulent flows in unstructured setups; (*c*) the inference of inflow and wall-thermal boundary conditions from scarce experimental measurements; (*d*) near-wall turbulence modeling in high-speed reacting boundary layers, including the prediction of skin friction and wall heating; (*e*) the quantification of associated uncertainties in the computational results with regard to both aleatoric and epistemic errors in input simulation parameters and physical models; and (*f*) the efficient deployment of multiphysics LES codes in massively parallel supercomputers.

The configurations in **Figure 5** have been the focus of recent LES investigations motivated by the availability of experimental data for validation. The typical grid sizes in these simulations are of order $\sim 0.1\text{--}100$ M elements, with $\sim 0.1\text{--}1$ M CPU hours required to compute a statistically significant number of flow-through times. For instance, simulations of UVa's scramjet configurations A and C have been performed by Fulton et al. (2012, 2013) that show good overall agreement with an extensive experimental data set and provide physical insight into dual-mode transition, supersonic mixing, and fuel jet interactions with wall-reflected shock waves from the compression ramp. Similarly, LES of the DLR scramjet have been carried out by Génin et al. (2003), Génin & Menon (2010a), Berglund & Fureby (2007), and Potturi & Edwards (2014), which have furthered the understanding of flame anchoring downstream of the injector wedge strut and found reasonable agreement with the experiments of Waidmann et al. (1994, 1995). Additionally, the simulations of the ONERA/JAXA configuration by Fureby et al. (2015) quantified the effects of alternating-wedge injection struts on mixing and combustion characteristics. The HiFIRE-2 simulations by Bermejo-Moreno et al. (2013) innovatively employed low-dissipation numerics along with an equilibrium wall model to treat near-wall turbulence in the boundary layers (**Figure 11**) and revealed large-scale oscillations of the shock train in the engine core that may have influences on the development of combustion dynamics. The HiFIRE-2 scramjet has also been computationally addressed by Saghafian et al. (2015a), who showed that the equilibrium wall model, in conjunction with the flamelet compressibility corrections for pressure and temperature described in Section 3.2.1, leads to improved agreement with the experiments of Cabell et al. (2011).

In addition to these breakthroughs, LES shows great potential to address aerothermal effects in scramjets that require longer analysis time windows than the maximum ones achievable in experimental test facilities, such as shock tunnels. In this regard, unstart in scramjets represents a case study where LES plays a relevant role in unveiling unsteady dynamics by exploiting higher spatiotemporal resolutions in comparison with predecessor RANS models.

3.2.3. Unstart in scramjet engines. As described in Section 1, the partial deceleration of the airflow captured in scramjet engines is produced by a number of shock waves that are generated externally along the compression ramps preceding the inlet and internally through oblique shocks from wall reflections and geometrical disturbances. An important technical barrier in the development of scramjets is the phenomenon of unstart, by which the internal system of shocks is unexpectedly expelled outside the engine in a short amount of time, preventing prompt corrective action on control surfaces or engine power and that can eventually cause loss of aircraft control. Perhaps the most famous illustration of this phenomenon in real supersonic flight, albeit in a different propulsion system, was encountered during the operation of the J-58 turboramjet engines in the SR-71 Blackbird at Mach 3 and was attributed to be the precursor of the disintegration of Blackbird tail number 952. Airframe roughness, loud banging, and sudden rolling and yawing

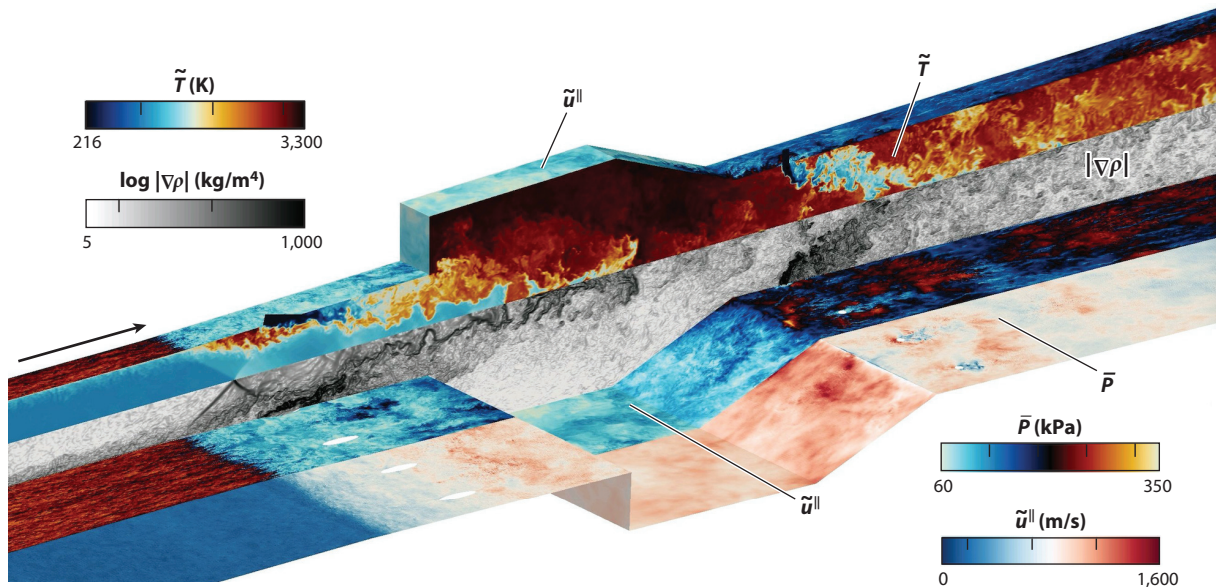


Figure 11

Wall-modeled large-eddy simulation of the HIFIRE-2 scramjet (see configuration schematics in **Figure 5a**) showing instantaneous isocontours of temperature, density gradient, pressure, and wall-parallel velocity at the exchange location with the wall model. Adapted with permission from Bermejo-Moreno et al. (2013).

were reportedly known products of asymmetric inlet unstart caused by too large pressures behind the terminal shock or by an excessive retraction of the inlet spike (USAF 1986).

In scramjets, a full unstart causes the flow in the entire engine to become subsonic (**Figure 12a**). As a result, the dynamic compression of the airflow occurs solely through external shock waves that create a large spillage of air around the inlet and a large increase in drag. The distortion of the shock train can be caused by (a) localized aerodynamic effects at the inlet, such as boundary-layer separation due to change in the angle of attack, and (b) strong pressure disturbances generated downstream in the combustor, which can be due to blockage produced by fuel injection and to thermal choking by excessive heat addition. The latter is the focus of this section because it overlaps with the topic of supersonic combustion.

The theory of 1D compressible inviscid flows predicts that when a cumulative amount of heat q per unit mass is added to a gas moving at supersonic speeds in a constant cross section duct, the static pressure increases and the Mach number decreases. For a critical amount of heat q_{\max} , which depends on the stagnation enthalpy and the Mach number upstream from the heat deposition zone, the gas velocity equals the local speed of sound and the duct becomes thermally choked. Further release of heat $q > q_{\max}$ requires a change of boundary conditions upstream for a steady solution to exist. The solution otherwise becomes a system of normal shocks moving away from the heat deposition zone so as to restore a steady Rayleigh flow solution, leaving subsonic flow behind.

Experimental visualizations by Laurence et al. (2013, 2015) of unstart in a model HyShot-2 scramjet tested at DLR's high-enthalpy shock tunnel have recently shown that, in real configurations, the description is much more complicated because the compression wave produced by thermal choking propagates upstream across a turbulent flow where mixing layers, fuel jets, boundary layers, and transonic regions significantly influence the 3D dynamics, which in

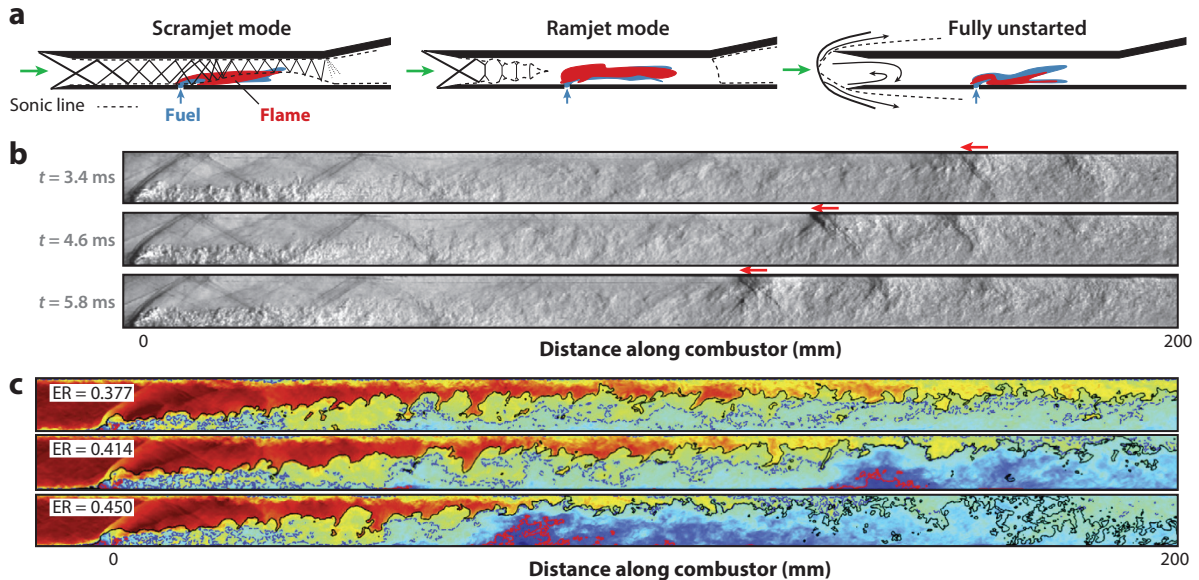


Figure 12

(a) Schematics of shock systems lines (*solid*) and sonic lines (*dashed*) in a notional dual-mode scramjet. (b) Schlieren sequence of unstart from shock-tunnel experiments of HyShot-2 at an equivalence ratio of 0.43, including the unstart shock train (*red arrows*) and test-time stamps. Adapted with permission from Laurence et al. (2015). (c) Instantaneous large-eddy simulation Mach number contours from -0.5 (*blue*) to 2.7 (*red*) in HyShot-2 along the midplane crossing the injector for three different equivalence ratios, corresponding to started (*top*) and unstarted cases (*middle* and *bottom*). Also included are the stoichiometric line (*solid black*) and the sonic line (*dashed blue*), showing the occurrence of combustion at supersonic velocities in the laboratory frame, along with a line that separates forward from reverse longitudinal flows (*red*). Adapted with permission from Larsson et al. (2015). Abbreviation: ER, equivalence ratio.

principle cannot be easily described by 1D homogeneous heat-deposition compressible-inviscid flow models. Unstart is initiated at a critical equivalence ratio $\gtrsim 0.40$ and gives rise to a shock train that moves upstream relatively slowly at speeds of order 10–100 m/s in comparison with the much faster forward flow at 1,850 m/s in the combustor (**Figure 12b**). The resulting unstart shock train comes to a halt downstream from the injector when the equivalence ratio is not too high, indicating a metastable configuration state that is yet to be understood. Accompanying numerical simulations by Laurence et al. (2013) and Larsson et al. (2015) demonstrated that the genesis of unstart is an excessive heat deposition local in the central-to-rear portion of the combustor within the supersonic flow. The local thermal choking is induced by a throat effect created by the combined action of the fuel injection, which increasingly displaces supersonic air streamlines towards the upper wall as the equivalence ratio increases (**Figure 12c**), and by heat addition, which primarily occurs along the air-rich streamlines because the stoichiometric proportions are always located closer to the oxidizer side of the mixing layers.

If the flow disturbance generated by the thermal choking is significant, the shock train creeps into the isolator. There, during an unstart event, the shock train creates strong adverse pressure gradients that lead to the separation of the sidewall turbulent boundary layers. The resulting structure is a pseudoshock that moves towards the inlet and eventually exits the engine. In dual-mode scramjets, the isolator is sufficiently long to confine and stabilize the pseudoshock when the downstream pressure disturbances are not too large, thereby enabling a safe transition from

scramjet to ramjet mode with subsonic and supersonic flows throughout the combustor and isolator, respectively (**Figure 12a**, center panel).

Recent computational analyses of unstart have been extended to the HIFiRE-2 configuration (Riley et al. 2016). Further analyses of unstart may be of interest, including reduced-order modeling based on LES results along with the deployment of flow control techniques to mitigate unstart and to formulate reliable procedures for engine restart.

4. CONCLUDING REMARKS AND FUTURE PROSPECTIVES

The large amount of research in recent years has increased our physical understanding of supersonic combustion. This review highlights only a very small portion of these breakthroughs. There are other relevant aspects of supersonic combustion in scramjets that are not addressed here, such as the emergence of plasma-assisted ignition methods for supersonic flows (Ju & Sun 2015) or the recent increase in the availability of highly resolved spatiotemporal data enabled by advances in experimental diagnostics like ultra-fast optics and tomography (Ma et al. 2015, Halls et al. 2016), which, in conjunction with theory and numerical simulations, can lead to substantial developments in this research field.

In most practical scramjet configurations, flame stabilization in scramjets often does not solely rely on lifted autoignition processes, particularly for heavy hydrocarbon fuels with long ignition times. Conversely, ignition and flameholding are achieved by shock-induced mechanisms or by flow sheltering in the form of recirculations enabled by appropriate injection configurations or side cavities. Once ignited, diffusion flames tend to persist in the combustor even under supersonic coflowing speeds, although shock impingements and multiscale compressibility effects caused by the high-speed turbulent relative motion between the fuel and oxidizer streams may alter the mixing dynamics and flame structures, which pose challenges in SGS modeling for LES of turbulent supersonic combustion.

Several aspects are worthy of future investigations. These include: (a) fundamental understanding of ignition, stabilization, and enhancement of flames in supersonic flows using plasma-based methods and shock-induced mechanisms; (b) development of SGS models for turbulent supersonic combustion, accounting for multiscale interactions in compressible turbulence along with chemical kinetics for advanced supersonic combustion hydrocarbon fuels; (c) study of supersonic combustion dynamics in flameholder cavities and their coupling with the overriding shear layer and shock train oscillations in the engine core; (d) investigation of directed energy deposition for forced ignition and relight of supersonic chemically reacting turbulent flows; (e) reduced-order modeling, control, and mitigation of unstart; (f) study of combustion physics at hypervelocities near the maximum-speed range of the scramjet flight corridor; and (g) integration of multiphysics SGS models in full-system simulations for verification, experimental validation, and predictive engineering analysis of scramjet engine performance under uncertainty.

Unprecedented levels of insight into air-breathing hypersonic propulsion have been gained by combining experiments, simulations, and theoretical modeling since the first review appeared in this journal on this topic 45 years ago (Ferri 1973). In particular, the role of flight experiments continues to be crucial for the development of this technical discipline. In the past, boldness and determination in experimentation and flight testing have often led humankind to the most important advances in aeronautics and astronautics, including the unparalleled accomplishments of Apollo, X-15, SR-71, and the late twentieth century stealth-aircraft programs. Similar decisiveness is paramount to the progress of hypersonic air-breathing propulsion technology. As Robert H. Goddard once expressed while testing rockets in the New Mexico desert: “Morning in the desert, when the impossible not only seems possible, but easy” (unpublished diary, February 6, 1937).

DISCLOSURE STATEMENT

The author is not aware of any biases that might be perceived as affecting the objectivity of this review.

ACKNOWLEDGMENTS

The author acknowledges funding from AFOSR grants FA9550-14-1-0219 and 1194592-1-TAAHO, managed by Dr. Chiping Li and Dr. Ivett Leyva, respectively. The author is also grateful to the Advanced Simulation and Computing Program (ASC) of the US Department of Energy's National Nuclear Security Administration (NNSA) for funding the Stanford PSAAP-I Center (2008–2013), grant DE-FC52-08NA28614, which was dedicated to the investigation of supersonic combustion in scramjets, and to all its participants.

LITERATURE CITED

- Barnes FW, Seagal C. 2015. Cavity-based flameholding for chemically-reacting supersonic flows. *Prog. Aerosp. Sci.* 76:24–41
- Berglund M, Fureby C. 2007. LES of supersonic combustion in a scramjet engine model. *Proc. Combust. Inst.* 31:2497–504
- Bermejo-Moreno I, Larsson J, Bodart J, Vicquelin R. 2013. Wall-modeled large-eddy simulations of the HIFiRE-2 scramjet. In *Annual Research Briefs 2013*, pp. 3–19. Stanford, CA: Cent. Turbul. Res.
- Berry S, Daryabeigi K, Wurster K, Bittner R. 2010. Boundary-layer transition on X-43A. *J. Spacecr. Rocket.* 47:922–44
- Bowcutt K, Paull A, Dolvin D, Smart M. 2012. *HIFiRE: an international collaboration to advance the science and technology of hypersonic flight*. Presented at Int. Congr. Aeronaut. Sci., 12th, Leiden, Neth.
- Boyce R, McIntyre T, O'Byrne S, Hagenmaier M. 2010. *Combustion scaling laws and inlet starting for Mach 8 inlet-injection radical farming scramjets*. Rep. AOARD-094019, Wright Patterson Airf. Base, OH
- Brieschenk S, O'Byrne S, Kleine H. 2013. Laser-induced plasma ignition studies in a model scramjet engine. *Combust. Flame* 160:145–48
- Brummund U, Nuding J. 1997. *Interaction of a compressible shear layer with shock waves: an experimental study*. Presented at Aerosp. Sci. Meet., 35th, Reno, NV, AIAA Pap. 1997-0392
- Burke SP, Schumann TEW. 1928. Diffusion flames. *Ind. Eng. Chem.* 20:998–1004
- Cabell K, Haas N, Storch A, Gruber M. 2011. *HIFiRE Direct-Connect Rig (HDCR) phase I scramjet test results from the NASA Langley Arc-Heated Scramjet Test Facility*. Presented at Int. Space Planes Hypersonic Syst. Technol. Conf., 17th, San Francisco, CA, AIAA Pap. 2011-248
- Cantu LML, Gallo ECA, Cutler AD, Danehy PM, Johansen CT, et al. 2016. *OH PLIF visualization of a premixed ethylene-fueled dual-mode scramjet combustor*. Presented at AIAA Aerosp. Sci. Meet., 54st, San Diego, CA, AIAA Pap. 2016-1763
- Chapuis M, Fedina E, Fureby C, Hannemann K, Karl S, Schramm JM. 2013. A computational study of the HyShot II combustor performance. *Proc. Combust. Inst.* 31:2101–9
- Cheng TS, Wehrmeyer JA, Pitz RW, Jarrett O, Northam GB. 1994. Raman measurement of mixing and finite-rate chemistry in a supersonic hydrogen-air diffusion flame. *Combust. Flame* 99:157–73
- Curran ET, Heiser WH, Pratt DT. 1996. Fluid phenomena in scramjet combustion systems. *Annu. Rev. Fluid Mech.* 28:323–60
- Curran ET, Murthy SNB, eds. 2000. *Scramjet Propulsion*. Reston, VA: Am. Inst. Aeronaut. Astronaut.
- Da Riva I, Urrutia JL. 1968. Ignition delay in diffusive supersonic combustion. *AIAA J.* 6:2095–53
- Del Álamo G, Williams FA, Sánchez AL. 2004. Hydrogen-oxygen induction times above crossover temperatures. *Combust. Sci. Technol.* 176:1599–626
- Doran EM. 2011. *A multi-dimensional flamelet model for ignition in multi-feed combustion systems*. PhD Thesis, Stanford Univ.

- Etheridge S, Lee JG, Carter C, Hagenmaier M. 2012. *Characterization of supersonic flow interaction with a shockwave using laser-based diagnostics*. Presented at AIAA/ASME/SAE/ASEE Joint Propuls. Conf. Exhib., 48th, Atlanta, GA, AIAA Pap. 2012-3776
- Ferrer PJ, Lehnasch G, Mura A. 2017. Compressibility and heat release effects in high-speed reactive mixing layers II. Structure of the stabilization zone and modeling issues relevant to turbulent combustion in supersonic flows. *Combust. Flame* 180:304–20
- Ferri A. 1973. Mixing-controlled supersonic combustion. *Annu. Rev. Fluid Mech.* 5:301–38
- Fulton J, Edwards J, Hassan H, McDaniel J, Goyne C, Rockwell R. 2013. *Continued hybrid LES/RANS simulation of a hypersonic dual-mode scramjet combustor*. Presented at AIAA Aerosp. Sci. Meet., 51st, Grapevine, TX, AIAA Pap. 2013-0117
- Fulton J, Edwards J, Hassan H, Rockwell R, Goyne C, et al. 2012. *Large-eddy/Reynolds-averaged Navier-Stokes simulation of a dual-mode scramjet combustor*. Presented at AIAA Aerosp. Sci. Meet., 50th, Nashville, TN, AIAA Pap. 2012-0115
- Fureby C. 2012. *LES for supersonic combustion*. Presented at AIAA Int. Space Planes Hypersonic Syst. Technol. Conf., 18th, Tours, France, AIAA Pap. 2012-5979
- Fureby C, Nordin-Bates K, Petterson K, Bresson A, Sabelnikov V. 2015. A computational study of supersonic combustion in strut injector and hypermixer flow fields. *Proc. Combust. Inst.* 35:2127–35
- Gamba M, Mungal GD. 2015. Ignition, flame structure and near-wall burning in transverse hydrogen jets in supersonic crossflow. *J. Fluid Mech.* 780:226–73
- Gardner AD, Hannemann K, Pauli A, Steelant J. 2005. Ground testing of the HyShot supersonic combustion flight experiment in HEG. *Shock Waves: Proc. Int. Symp. Shock Waves*, 24th, 11–16 July, Beijing, China, ed. Z Jiang, pp. 329–34. Berlin: Springer-Verlag
- Génin F, Chernyavsky B, Menon S. 2003. *Large eddy simulation of scramjet combustion using a subgrid mixing/combustion model*. Presented at Int. Space Planes Hypersonic Syst. Technol. Conf., 12th, Norfolk, VA, AIAA Pap. 2003-7035
- Génin F, Menon S. 2010a. Simulation of turbulent mixing behind a strut injector in supersonic flow. *AIAA J.* 3:526–39
- Génin F, Menon S. 2010b. Studies of shock/turbulent shear layer interaction using large-eddy simulation. *Comput. Fluids* 39:800–19
- Giovangigli V. 1991. *Multicomponent Flow Modeling*. Basel, Switz.: Birkhäuser
- Gonzalez-Juez ED, Kerstein AR, Ranjan R, Menon S. 2017. Advances and challenges in modeling high-speed turbulent combustion in propulsion systems. *Prog. Energy Combust. Sci.* 60:26–67
- Goyne CP, Krauss RH, McDaniel JC, Whitehurst WB. 2007. Test gas vitiation effects in a dual-mode scramjet combustor. *J. Propuls. Power* 31:36–53
- Goyne CP, Rodriguez CP, McClinton CR. 2006. Experimental and numerical study of a dual-mode scramjet combustor. *J. Propuls. Power* 22:481–89
- Gradya NR, Pitz RW, Carter CD, Hsu KY. 2016. Raman scattering measurements of mixing and finite-rate chemistry in a supersonic reacting flow over a piloted ramped cavity. *Combust. Flame* 165:310–20
- Gruber MR, Donbar JM, Carter CD, Hsu KY. 2004. Mixing and combustion studies using cavity-based flameholders in a supersonic flow. *J. Propuls. Power* 20:769–78
- Hallion RP, ed. 1987. *The Hypersonic Revolution*, Vol. 2: *From Scramjet to the National Aero-Space Plane (1964–1986)*. Wright Patterson Airf. Base, OH: Aeronaut. Syst. Div.
- Hallion RP, Bedke CM, Schanz MV. 2016. *Hypersonic Weapons and US National Security: A 21st Century Breakthrough*. Arlington, VA: Mitchell Inst. Aerosp. Stud.
- Halls BR, Gord JR, Jiang N, Splichenko M, Roy S, Meyer TR. 2016. *High-speed three-dimensional tomographic measurements for combustion systems*. Presented at AIAA Aerodyn. Meas. Technol. Ground Test. Conf., 32nd, Washington, DC, AIAA Pap. 2016-4027
- Hank JM, Murphy JS, Murtzman RC. 2008. *The X-51A scramjet engine flight demonstration program*. Presented at AIAA Int. Space Planes Hypersonic Syst. Technol. Conf., 15th, Dayton, OH, AIAA Pap. 2008-2540
- Heiser WH, Pratt DT. 1994. *Hypersonic Airbreathing Propulsion*. Washington, DC: Am. Inst. Aeronaut. Astronaut.
- Hermanson JC, Cetegen BM. 2000. Shock-induced mixing of nonhomogeneous density turbulent jets. *Phys. Fluids* 12:1210–25

- Hermanson JC, Dimotakis PE. 1989. Effects of heat release in a turbulent, reacting shear layer. *J. Fluid Mech.* 199:333–75
- Hirschfelder J, Curtiss CF, Bird RB. 1954. *Molecular Theory of Gases and Liquids*. New York: Wiley
- Hong Z, Davidson DF, Hanson RK. 2011. An improved H₂/O₂ mechanism based on recent shock tube/laser absorption measurements. *Combust. Flame* 158:633–44
- Huete C, Sánchez AL, Williams FA. 2017. Diffusion-flame ignition by shock-wave impingement on a hydrogen-air supersonic mixing layer. *J. Propuls. Power* 33:256–63
- Huete C, Sánchez AL, Williams FA, Urzay J. 2015. Diffusion-flame ignition by shock-wave impingement on supersonic mixing layers. *J. Fluid Mech.* 784:74–108
- Huete C, Urzay J, Sánchez AL, Williams FA. 2016. Weak-shock interactions with transonic laminar mixing layers of fuels for high-speed propulsion. *AIAA J.* 54:962–75
- Huzel DK. 1962. *From Peenemünde to Canaveral*. Englewood Cliffs, NJ: Prentice-Hall
- Ihme M, See YC. 2011. Prediction of autoignition in a lifted methane/air flame using an unsteady flamelet/progress variable model. *Combust. Flame* 157:1850–62
- Jackson KR, Gruber MR, Buccellaturo S. 2014. Mach 6–8+ hydrocarbon-fueled scramjet flight experiment: the HIFiRE Flight 2 project. *J. Propuls. Power* 31:36–53
- Jackson TL, Kapila AK. 1985. Shock-induced thermal runaway. *SIAM J. Appl. Math.* 45:130–37
- Ju Y, Sun W. 2015. Plasma assisted combustion: dynamics and chemistry. *Prog. Energy Combust. Sci.* 48:21–83
- Kee RJ, Dixon-Lewis G, Warnatz J, Coltrin ME, Miller JA. 1986. *A Fortran computer code package for the evaluation of gas-phase multicomponent transport properties*. Tech. Rep. SAND-86-8246, Sandia Natl. Lab., Albuquerque, NM
- Kirik JW, Goyne CP, Peltier SJ, Carter CD, Hagenmaier MA. 2014. Velocimetry measurements of a scramjet cavity flameholder with inlet distortion. *J. Propuls. Power* 30:1568–76
- Knudsen E, Pitsch H. 2009. A general flamelet transformation useful for distinguishing between premixed and non-premixed modes of combustion. *Combust. Flame* 156:678–96
- Koo H, Donde P, Raman V. 2011. A quadrature-based LES/transported probability density function approach for modeling supersonic combustion. *Proc. Combust. Inst.* 31:2203–10
- Larsson J, Laurence SJ, Bermejo-Moreno I, Bodart J, Karl SK, Vicquelin R. 2015. Incipient thermal choking and stable shock-train formation in the heat-release region of a scramjet combustor. Part II: large-eddy simulations. *Combust. Flame* 162:907–20
- Laurence SJ, Karl S, Martinez-Schramm J, Hannemann K. 2013. Transient fluid-combustion phenomena in a model scramjet. *J. Fluid Mech.* 722:85–120
- Laurence SJ, Lieber D, Martinez Schramm J, Hannemann K, Larsson J. 2015. Incipient thermal choking and stable shock-train formation in the heat-release region of a scramjet combustor. Part I: shock-tunnel experiments. *Combust. Flame* 161:921–31
- Lee S, Lele SK, Moin P. 1991. Eddy shocklets in decaying compressible turbulence. *Phys. Fluids* 3:657–64
- Leyva IA. 2017. The relentless pursuit of hypersonic flight. *Phys. Today* 70(11):30–36
- Li C, Kailasanath K, Oran ES. 1994. Detonation structures behind oblique shocks. *Phys. Fluids* 6:1600–11
- Lighthill MJ. 1950. Reflection at a laminar boundary layer of a weak steady disturbance to a supersonic stream, neglecting viscosity and heat conduction. *Q. J. Mech. Appl. Math.* 54:303–25
- Lifnán A. 1974. The asymptotic structure of counterflow diffusion flames for large activation energies. *Acta Astronaut.* 1:1007–39
- Lifnán A, Crespo A. 1976. An asymptotic analysis of unsteady diffusion flames for large activation energies. *Combust. Sci. Technol.* 14:95–117
- Lifnán A, Urrutia JL, Fraga E. 1966. On diffusive supersonic combustion. *Proc. Int. Counc. Aeronaut. Sci. Congr., 4th, London, UK, 12–16 Sept.*, ed. J Bradbrooke, J Bruce, RR Dexter, pp. 607–18. London: Macmillan
- Lifnán A, Vera M, Sánchez AL. 2015. Ignition, liftoff, and extinction of gaseous diffusion flames. *Annu. Rev. Fluid Mech.* 47:293–314
- Liu JT, Rieker GB, Jeffries JB, Gruber MR, Carter CD, et al. 2005. Near-infrared diode laser absorption diagnostic for temperature and water vapor in a scramjet combustor. *Appl. Opt.* 44:6701–11

- Lorrain P, Brieschenk S, Capra B, Boyce R. 2012. *A detailed investigation of nominally 2D radical-farming scramjet combustion*. Presented at AIAA Int. Space Planes Hypersonic Syst. Technol. Conf., 18th, Tours, France, AIAA Pap. 2012-5812
- Ma L, Lei Q, Wu Y, Ombrello TM, Carter CD. 2015. 3D measurements of ignition processes at 20 kHz in a supersonic combustor. *Appl. Phys. B* 119:313–21
- Mahle I, Foysi H, Sarkar S, Friedrich R. 2007. On the turbulence structure in inert and reacting compressible mixing layers. *J. Fluid Mech.* 25:171–80
- Mai T, Sakimitsu Y, Nakamura H, Ogami Y, Kudo T, Kobayashi H. 2011. Effect of the incident shock wave interacting with transversal jet flow on the mixing and combustion. *Proc. Combust. Inst.* 33:2335–42
- Marble FE. 1994. Gasdynamic enhancement of nonpremixed combustion. *Int. Symp. Combust.* 24:1–12
- Marshall LA, Bahm C, Corpene GF, Sherrill R. 2005. *Overview with results and lessons learned of the X-43A Mach 10 flight*. Presented at AIAA Int. Space Planes Hypersonic Syst. Technol. Conf., 13th, Capua, Italy, AIAA Pap. 2005-3336
- Mathur T, Gruber M, Jackson K, Donbar J, Donaldson W, Jackson T. 2001. Supersonic combustion experiments with a cavity-based fuel injector. *J. Propuls. Power* 17:1305–12
- Mathur T, Lin KC, Kennedy P, Gruber M, Donbar J, et al. 2000. Liquid JP-7 combustion in a scramjet combustor. Presented at AIAA/ASME/SAE/ASEE Joint Propuls. Conf. Exhib., Las Vegas, NV, AIAA Pap. 2000-3581
- McBride BJ, Gordon S, Reno MA. 2005. *Coefficients for calculating thermodynamic and transport properties of individual species*. NASA Tech. Memo. 4513, Natl. Aeronaut. Space Admin., Washington, DC
- McClinton C. 2006. *X-43-Scramjet power breaks the hypersonic barrier: Dryden lectureship in research*. Presented at AIAA Aerosp. Sci. Meet. Exhib., 44th, Reno, NV, AIAA Pap. 2006-1
- McDaniel J, Goyne C, Edwards JR, Chelliah H, Cutler A, Givi P. 2009. *US National Center for Hypersonic Combined Cycle Propulsion: an overview*. Presented at AIAA Int. Space Planes Hypersonic Syst. Technol. Conf., 16th, Bremen, Germany, AIAA Pap. 2009-7280
- McGuire J, Boyce R, Mudford N. 2008. Radical farm ignition processes in two-dimensional supersonic combustion. *J. Propuls. Power* 24:1248–57
- McRae CD, Johansen CT, Danehy PM, Gallo ECA, Cantu L, et al. 2013. *OH PLIF visualization of the UVa supersonic combustion experiment: configuration C*. Presented at AIAA Aerosp. Sci. Meet., 51st, Grapevine, TX, AIAA Pap. 2013-0034
- Mellado JD, Sánchez AL, Kim JS, Liñán A. 2000. Branched-chain ignition in strained mixing layers. *Combust. Theor. Model.* 4:265–88
- Micka DJ, Driscoll JF. 2009. Combustion characteristics of a dual-mode scramjet combustor with cavity flameholder. *Proc. Combust. Inst.* 32:2397–404
- Middha P, Yang B, Wang H. 2002. A first-principle calculation of the binary diffusion coefficients pertinent to kinetic modeling of H₂/O₂/He flames. *Proc. Combust. Inst.* 29:1361–69
- Miller RS, Madnia CK, Givi P. 1994. Structure of a turbulent reacting mixing layer. *Combust. Sci. Technol.* 99:1–36
- Morris CI, Kamel MR, Hanson RK. 1998. Shock-induced combustion in high-speed wedge flows. *Int. Symp. Combust.* 27:2157–64
- Natl. Res. Coun. 2008. *U.S. Conventional Prompt Global Strike: Issues for 2008 and Beyond*. Washington, DC: Natl. Acad.
- O'Brien J, Urvay J, Ihme M, Moin P, Saghafian A. 2014. Subgrid-scale backscatter in reacting and inert supersonic hydrogen-air turbulent mixing layers. *J. Fluid Mech.* 743:554–84
- Odum J, Paull A. 2007. Radical farming in scramjets. In *New Results in Numerical and Experimental Fluid Mechanics*, ed. C Tropea, SJakirlic, H Heinemann, R Henke, H Hönlinder, pp. 276–83. Berlin: Springer-Verlag
- Ombrello T, Blunck DL, Resor M. 2016. Quantified infrared imaging of ignition and combustion in a supersonic flow. *Exp. Fluids* 57:140–52
- Ombrello T, Peltier S, Carter CD. 2015. *Effects of inlet distortion on cavity ignition in supersonic flow*. Presented at AIAA Aerosp. Sci. Meet., 53rd, Kissimmee, FL, AIAA Pap. 2015-0082
- Papamoschou D, Roshko A. 1988. The compressible turbulent shear layer: an experimental study. *J. Fluid Mech.* 197:453–77

- Paull A, Frost M, Alesi H. 2000. *HyShot-T4 supersonic combustion experiments*. NASA Tech. Rep. NAG-1-2113, Univ. Queensland, Brisbane, Aust.
- Pecnik R, Terrapon VE, Ham F, Iaccarino G, Pitsch H. 2012. Reynolds-averaged Navier–Stokes simulations of the HyShot II scramjet. *AIAA J.* 50:1717–32
- Pellett GL, Vaden SN, Wilson LG. 2008. *Gaseous surrogate hydrocarbons for a HIFiRE scramjet that mimic opposed jet extinction limits for cracked JP fuels*. Presented at JANNAF Propuls. Meet., 55th, Boston, MA
- Peters N. 2000. *Turbulent Combustion*. Cambridge, UK: Cambridge Univ. Press
- Pierce CD, Moin P. 1998. A dynamic model for subgrid-scale variance and dissipation rate of a conserved scalar. *Phys. Fluids* 10:3041–44
- Pierce CD, Moin P. 2004. Progress-variable approach for large-eddy simulation of non-premixed turbulent combustion. *J. Fluid Mech.* 504:73–97
- Potturi AS, Edwards JR. 2014. Hybrid large-eddy/Reynolds-averaged Navier–Stokes simulations of flow through a model scramjet. *AIAA J.* 52:1417–29
- Pratt DT, Humphrey JW, Glenn DE. 1991. Morphology of standing oblique detonation waves. *J. Propuls. Power* 7:837–45
- Rhodes RP, Rubins PM, Chriss DE. 1962. *The effect of heat release on the flow parameters in shock-induced combustion*. Rep. AEDC-TDR-62-7S, Arnold Airf. Base, TN
- Riley LP, Hagenmaier MA, Donbar JM, Gaitonde DV. 2016. *A computational investigation of unstart in a dual-mode scramjet*. Presented at AIAA Sci. Technol. Forum Expo., 54th, San Diego, CA, AIAA Pap. 2016-1191
- Rubins PM, Bauer RC. 1994. Review of shock-induced supersonic combustion research and hypersonic applications. *J. Propuls. Power* 10:593–601
- Saghafian A. 2014. *High-fidelity simulations and modeling of compressible reacting flows*. PhD Thesis, Stanford Univ.
- Saghafian A, Shunn L, Philips DA, Ham F. 2015a. Large eddy simulations of the HIFiRE scramjet using a compressible flamelet/progress variable approach. *Proc. Combust. Inst.* 35:2163–72
- Saghafian A, Terrapon VE, Pitsch H. 2015b. An efficient flamelet-based combustion model for compressible flows. *Combust. Flame* 162:652–67
- Samtaney R, Pullin DI, Kosovic B. 2001. Direct numerical simulation of decaying compressible turbulence and shocklet statistics. *Phys. Fluids* 13:1415–30
- Sánchez AL, Balakrishnan G, Liñán A, Williams FA. 1996. Relationships between bifurcation and numerical analyses for ignition of hydrogen-air diffusion flames. *Combust. Flame* 105:569–90
- Sánchez AL, Williams FA. 2014. Recent advances in understanding of flammability characteristics of hydrogen. *Prog. Energy Combust. Sci.* 41:1–55
- Scherrer D, Dessornes O, Ferrier M, Vincent-Randonnier A, Sabel'nikov V. 2016. Research on supersonic combustion and scramjet combustors at ONERA. *Aerosp. Lab* 11:04
- Shan F, Hou L, Chen Z, Chen J, Wang L. 2017. Linearized correction to a flamelet-based model for hydrogen-fueled supersonic combustion. *Int. J. Hydrogen Energy* 42:11937–44
- Smart MK, Hass NE, Paull A. 2006. Flight data analysis of the HyShot 2 scramjet flight experiment. *AIAA J.* 44:2366–75
- Smart MK, Stalker R, Morgan R, Paull A. 2008. Hypersonics research in Australia. In *Advances on Propulsion Technology for High-Speed Aircraft*, RTO-EN-AVT-150, Pap. 11, pp. 1–30. Neuilly-sur-Seine, Fr.: RTO
- Stewartson K, Williams PG. 1969. Self-induced separation. *Proc. R. Soc. A* 312:181–206
- Tirtey S, Boyce R, Brown M, Capra B, Creagh M, et al. 2014. SCRAMSPACE: radical-farming scramjet for access to space. In *Hypersonic Flight Testing*, STO-EN-AVT-234, Pap. 11, pp. 1–31. Rhode Saint Genèse, Belg.: Von Karman Inst. Fluid Dyn.
- Tuttle SG, Carter CD, Shu KY. 2014. Particle image velocimetry in a non-reacting and reacting high-speed cavity. *J. Propuls. Power* 30:576–91
- Urzay J, Kseib N, Davidson DF, Iaccarino G, Hanson RK. 2014. Uncertainty-quantification analysis of the effects of residual impurities on hydrogen-oxygen ignition in shock tubes. *Combust. Flame* 161:1–15
- Urzay J, Kseib N, Palacios F, Larsson J, Iaccarino G. 2012. A stochastic flamelet progress-variable approach for numerical simulations of high-speed turbulent combustion under chemical-kinetic uncertainties. In *Annual Research Briefs 2012*, pp. 14–27. Stanford, CA: Cent. Turbul. Res.

- USAF (US Airf.). 1986. *SR-71A Flight manual*. Norton Airf. Base, CA
- Waidmann W, Alff F, Brummund U, Böhm M, Clauss W, Oschwald M. 1994. *Experimental investigation of the combustion process in a supersonic combustion ramjet (scramjet)*. DGLR Jahrestag. Rep. 94-E3-084, DGLR, Bonn, Ger.
- Waidmann W, Brummund U, Nuding J. 1995. Experimental investigation of supersonic ramjet combustion (scramjet). *Proc. Int. Symp. Transp. Phenom. Combust.*, 8th, San Francisco, Calif., 16–20 July, ed. SH Chen, pp. 1473–84. Washington, DC: Taylor & Francis
- Walker S, Sherk J, Shell D, Schena R, Bergmann JF, Gladback J. 2008. *The DARPA/AF Falcon program: the hypersonic technology vehicle #2 (HTV-2) flight demonstration phase*. Presented at AIAA Int. Space Planes Hypersonic Syst. Technol. Conf., 15th, Dayton, OH, AIAA Pap. 2008-2539
- Wang H, You X, Joshi AV, Davis SG, Laskin A, et al. 2007. *USC mech version II. High-temperature combustion reaction model of H₂/CO /C₁-C₄ compounds*. Combust. Kinet. Lab., Univ. South. Calif., Los Angeles, CA. http://ignis.usc.edu/USC_Mech_II.htm
- Watts JD. 1968. *Flight experience with shock impingement and interference heating on the X-15-A2 research airplane*. NASA Tech. Memo. X-1669, Natl. Aeronaut. Space Admin., Washington, DC
- Woolf AF. 2016. *Conventional prompt global strike and long-range ballistic missiles: background and issues*. Tech. Rep. R41464, US Congr. Res. Serv., Washington, DC
- Xu R, Chen D, Wang K, Tao Y, Shao JK, et al. 2017. *HyChem model: application to petroleum-derived jet fuels*. Presented at U.S. Natl. Combust. Meet., 10th, College Park, MD
- Zeman O. 1990. Dilatation dissipation: the concept and application in modeling compressible mixing layers. *Phys. Fluids* 2:178–88

Contents

John Leask Lumley: Whither Turbulence? <i>Sidney Leibovich and Zellman Warhaft</i>	1
Agitation, Mixing, and Transfers Induced by Bubbles <i>Frédéric Riso</i>	25
Numerical Models of Surface Tension <i>Stéphane Popinet</i>	49
Some Recent Developments in Turbulence Closure Modeling <i>Paul A. Durbin</i>	77
Diffuse-Interface Capturing Methods for Compressible Two-Phase Flows <i>Richard Saurel and Carlos Pantano</i>	105
Instabilities of Internal Gravity Wave Beams <i>Thierry Dauxois, Sylvain Joubaud, Philippe Odier, and Antoine Venaille</i>	131
Hydraulic Mineral Waste Transport and Storage <i>Lionel Pullum, David V. Boger, and Fiona Sofra</i>	157
Fire Whirls <i>Ali Tobidi, Michael J. Gollner, and Huabua Xiao</i>	187
High Explosive Detonation–Confiner Interactions <i>Mark Short and James J. Quirk</i>	215
Slamming: Recent Progress in the Evaluation of Impact Pressures <i>Frédéric Dias and Jean-Michel Ghidaglia</i>	243
Double-Diffusive Convection at Low Prandtl Number <i>Pascale Garaud</i>	275
Microstructural Dynamics and Rheology of Suspensions of Rigid Fibers <i>Jason E. Butler and Braden Snook</i>	299
Nonlinear Nonmodal Stability Theory <i>R.R. Kerswell</i>	319
Intracellular Fluid Mechanics: Coupling Cytoplasmic Flow with Active Cytoskeletal Gel <i>Alex Mogilner and Angelika Manhart</i>	347

Active and Passive Microrheology: Theory and Simulation <i>Roseanna N. Zia</i>	371
Particle Segregation in Dense Granular Flows <i>John Mark Nicholas Timm Gray</i>	407
The Sound of Flow Over Rigid Walls <i>William Devenport, Nathan Alexander, Stewart Glegg, and Meng Wang</i>	435
Lymphatic System Flows <i>James E. Moore Jr. and Christopher D. Bertram</i>	459
Microfluidics to Mimic Blood Flow in Health and Disease <i>Bernhard Sebastian and Petra S. Dittrich</i>	483
Hydrodynamic Interactions Among Bubbles, Drops, and Particles in Non-Newtonian Liquids <i>R. Zenit and J.J. Feng</i>	505
Wall-Modeled Large-Eddy Simulation for Complex Turbulent Flows <i>Sanjeeb T. Bose and George Ilhwan Park</i>	535
Rheology of Active Fluids <i>David Saintillan</i>	563
Supersonic Combustion in Air-Breathing Propulsion Systems for Hypersonic Flight <i>Javier Urzay</i>	593
Elastocapillarity: When Surface Tension Deforms Elastic Solids <i>José Bico, Étienne Reyssat, and Benoît Roman</i>	629
Sensitivity and Nonlinearity of Thermoacoustic Oscillations <i>Matthew P. Juniper and R.I. Sujith</i>	661
Instabilities in Blistering <i>Anne Juel, Draga Pihler-Puzović, and Matthias Heil</i>	691

Indexes

Cumulative Index of Contributing Authors, Volumes 1–50	715
Cumulative Index of Article Titles, Volumes 1–50	725

Errata

An online log of corrections to *Annual Review of Fluid Mechanics* articles may be found at <http://www.annualreviews.org/errata/fluid>